Original paper

TETGAR_C: a novel three-dimensional (3D) provenance plot and calculation tool for detrital garnets

Wolfgang KNIERZINGER[1*], Michael WAGREICH[1], Franz KIRALY[2], Eun Young LEE[3], Theodoros NTAFLOS[2]

[1] *University of Vienna, Department of Geodynamics and Sedimentology, Althanstrasse 14, 1090 Vienna, Austria; wolfgang.knierzinger@univie.ac.at*

[2] *University of Vienna, Department of Lithospheric Research, Althanstrasse 14, 1090 Vienna, Austria*

[3] *Chonnam National University, Faculty of Earth Systems and Environmental Sciences, 33 Yongbong-no, Bukgu, Gwangju 61186, Republic of Korea*

[*] *Corresponding author*

This paper presents a new interactive MATLAB-based visualization and calculation tool (TETGAR_C) for assessing the provenance of detrital garnets in a four-component (tetrahedral) plot system (almandine–pyrope–grossular–spessartine). Based on a freely-accessible database and additional electron-microprobe data, the chemistry of more than 2,600 garnet samples was evaluated and used to create various subfields in the tetrahedron that correspond to calc-silicate rocks, felsic igneous rocks (granites and pegmatites) as well as metasedimentary and metaigneous rocks of various metamorphic grades. These subfields act as reference structures facilitating assignments of garnet chemistries to source lithologies. An integrated function calculates whether a point is located in a subfield or not. Moreover, TETGAR_C determines the distance to the closest subfield's mean value. Compared with conventional ternary garnet discrimination diagrams, this provenance tool enables a more accurate assessment of potential source rocks by reducing the overlap of specific subfields and offering quantitative testing of garnet compositions. In particular, a much clearer distinction between garnets from greenschist-facies rocks, amphibolite-facies rocks, blueschist-facies rocks and felsic igneous rocks is achieved. Moreover, TETGAR_C enables a distinction between garnet grains with metaigneous and metasedimentary provenance. In general, metaigneous garnet tends to have higher grossular content than metasedimentary garnet formed under similar P–T conditions.

1. Introduction

Garnets are very abundant in metamorphic rocks and also occur as primary magmatic minerals in igneous rocks (Hieptas 2012). Furthermore, they are quite common components of siliciclastic sediments (Boggs 2009) and relatively stable during sediment transport and diagenesis (Morton et al. 2004; Morton and Hallsworth 2007; Garzanti et al. 2015).

For that reason, detrital single garnet grain analysis in combination with heavy-mineral analysis and analysis of weathering features provides vital information on erosional processes helping to reconstruct the temporal and spatial evolution of peri-orogenic sedimentary basins (e.g., Win et al. 2007; von Eynatten and Dunkl 2012; Stutenbecker et al. 2017; Hülscher et al. 2018; Caracciolo et al. in print). As studies imply, chemical differences of detrital garnets are often due to different grain size distributions of garnets in host rocks (Krippner et al. 2015, 2016).

Garnet chemistry holds considerable importance in the field of sedimentary provenance analysis (e.g., Zemann 1962; Morton 1985; Deer et al. 1992; Takeuchi 1994; Andò et al. 2014). In this respect, several discrimination diagrams and discrimination approaches have been developed enabling allocation of the chemistry of garnet to specific source rocks (e.g., Wright 1938; Teraoka et al. 1997; Preston et al. 2002; Schulze 2003; Grütter et al. 2004; Mange and Morton 2007; Méres 2008; Aubrecht et al. 2009; Suggate and Hall 2014; Hardman et al. 2018; Tolosano-Delgado et al. 2018). A detailed assessment of advantages and disadvantages of most of these discrimination tools can be found in Krippner et al. (2014). Regarding these ternary discrimination diagrams, Krippner et al. (2014) concluded a relatively low (< 50%) success rate for an unambiguous classification of garnet for several groups such as metaigneous and metasedimentary amphibolites or metaigneous and metasedimentary granulites.

In order to overcome some of the shortcomings of conventional garnet discrimination diagrams, this paper

introduces a new MATLAB-based visualization and discrimination tool (TETGAR_C) – a three-dimensional end-member plot combined with a quantitative interpretation of the garnet origin.

Centred on a case study built upon chemical data of garnet from Miocene sediments in Lower and Upper Austria, a comparison is made between ternary garnet discrimination diagrams of Preston et al. (2002), Mange and Morton (2007), Méres (2008) and Aubrecht et al. (2009) on the one hand and the new TETGAR_C discrimination tool on the other.

2. Garnet discrimination

2.1. Garnet chemistry

According to the mineralogical nomenclature of Grew et al. (2013), the garnet supergroup includes minerals with the formula $A_3B_2C_4O_{12}$, irrespective of the elements that occupy the four atomic sites. Depending on the bulk-rock composition and P–T conditions, garnets incorporate different elements in the A, B and C positions of the crystal lattice during formation and growth (Mange and Morton 2007; Andò et al. 2014).

Chemically, the vast majority of all garnet compositions can be expressed by five end-members: almandine ($Fe_3Al_2[SiO_4]_3$), pyrope ($Mg_3Al_2[SiO_4]_3$), spessartine ($Mn_3Al_2[SiO_4]_3$), grossular ($Ca_3Al_2[SiO_4]_3$) and andradite ($Ca_3Fe^{3+}_2[SiO_4]_3$) (Deer et al. 1982; Mange and Morton 2007). It shall be noted that compositional differences in garnets are driven by both thermodynamics and fractional crystallization (Kohn 2003). Almandine, the most common garnet endmember, mainly appears in regionally metamorphosed schists and gneisses. Its formation requires a relatively high-Al educt (Deer et al. 1982; Mange and Morton 2007; Suggate and Hall 2014). A typical paragenesis of almandine in micaschist includes biotite, muscovite, chlorite and quartz, sometimes kyanite and staurolite (Pichler and Schmitt-Riegraf 1993). Almandine is also found in many volcanic rocks, including andesite and dacite (e.g., Deer et al. 1982; Mange and Morton 2007; Suggate and Hall 2014).

Relatively high pyrope content is commonly attributed to granulites and eclogites (Mange and Morton 2007; Aubrecht et al. 2009; Suggate and Hall 2014).

At the upper border of the greenschist facies, spessartine can be formed at the expense of Mn-components of chlorites (Theye et al. 1996). Accordingly, almandine–spessartine-rich garnets are typical of greenschist-facies conditions (e.g., Brown 1969; Shenbao 1993; Paulick and Franz 2001; Willner et al. 2001; Makrygina and Suvorova 2011). Higher spessartine content is also typical of garnets in granitoid rocks and in blueschists (e.g.,

Okay 1980; Deer et al. 1982; Manning 1983; Suggate and Hall 2014).

Grossular is a characteristic component of metamorphosed impure calcareous rocks (Suggate and Hall 2014). Besides the dependency on sufficient contents of Ca in the host rock, the genesis of grossular-rich garnet is mostly associated with contact and regional metamorphism (e.g., Shimazki 1977; Sengupta and Raith 2002; Malvoisin et al. 2011; Antao 2013). Grossular–almandine-rich garnets are commonly attributed to high-P metasedimentary rocks (e.g., Deer et al. 1982; Oliver 2001; Ballèvre et al. 2003; Suggate and Hall 2014). Garnets of calc-silicate rocks are often dominated by the grossular–andradite solid solution (e.g., Deer et al. 1982; Suggate and Hall 2014).

Andradite and the rarer end-member schorlomite ($Ca_3Ti_2[(Si, Fe^{3+}, Fe^{2+})O_4]_3$) commonly occur associated in alkaline igneous rocks and skarns (Deer et al. 1982). Higher contents (> 5%) of the generally rare end-member uvarovite $Ca_3Cr_2(SiO_4)_3$ are usually confined to skarns, ores and ultramafic rocks (Suggate and Hall 2014).

2.2. Garnet provenance

Detailed quantitative analyses of detrital garnets in the context of provenance analysis were established already in the 1980's as sophisticated microanalytical tools, particularly electron-microprobe analysis, became widely available (Morton 1985; Morton 1987; Haughton and Farrow 1989; Mange and Morton 2007). In more recent years, considerable progress in the field has been made by implementing novel Raman spectroscopy techniques allowing quick and reliable identification of rarer anisotropic garnet end-members (e.g., Andò et al. 2009; Bersani et al. 2009; Andò and Garzanti 2014; Caracciolo et al. in print).

Chemical zoning of metamorphic garnets is a common feature that develops during mineral growth (Spear 1995). Variations of index elements such as Fe, Mg, Ca and Mn reflect the entire evolution of the rock including changes in P and T, mineral assemblages and heat flow, stress, strain, inter- and intragranular movement of rock material and fluid flow (Spear 1995; Kohn 2003). Usually, greenschist-facies garnets show stronger zoning than those of higher metamorphic conditions. Progressive depletion of Mn towards the rim results in a bell-shaped distribution of spessartine, indicating greenschist- or amphibolite-facies conditions during prograde metamorphism (Cooke et al. 2000; Schmolke et al. 2006). By contrast, retrograde garnets (inverse zoning) are usually characterized by an outward increase of Mn and a decrease of Mg (Dietvorst 1982). Growth zoning patterns are commonly obliterated in high-grade garnets by volume diffusion (Tuccillo et al. 1990).

Unlike detailed analyses of element-zoning patterns of garnets in source rocks, point analyses of detrital garnets only provide limited insights into the course of metamorphism, since a distinction between the core (older) and the rim (younger) cannot always be achieved. Relict (e.g., spessartine-rich almandines of granitoid origin in high-grade orthogneisses; see Vrána et al. 2009) and 'polymetamorphic' garnets (e.g., Faryad and Hoinkes 2004; Bestel et al. 2009) further complicate a correct classification of detrital garnets.

Despite many advances in recent years, an attribution of garnets to possible source rocks and metamorphic conditions remains a complicated and challenging task. To achieve best possible results, garnet provenance studies shall be conducted in a multidisciplinary fashion involving assessments of heavy-mineral assemblages, chemical analyses of various minerals (e.g., rutile, tourmaline, zircon, amphiboles, clays) and detailed characterizations of mineral grain sizes and weathering structures (e.g., Morton et al. 2004; Weltje and von Eynatten 2004; Win et al. 2007; Andò et al. 2012; Krippner et al. 2016).

2.3. Garnet discrimination approaches

Visualization of data in garnet discrimination diagrams inevitably means simplification and generalization since it is not possible to graphically represent all end-members of the garnet group. Focussing on the most frequently-occurring end-members almandine, pyrope, grossular and spessartine – as in most garnet discrimination approaches – provides a useful option for interpreting the provenance of many detrital garnets.

The classical garnet discrimination diagram of Preston et al. (2002; see also Wright 1938) divides garnets roughly into four petrological subfields (Fig. 1) associated with different source rocks: (1) granites

and (granite) pegmatites, (2) (biotite) micaschists, (3) amphibolites and (4) eclogites.

The garnet classification diagram of Mange and Morton (2007) enables a distinction of six types of garnets (Fig. 2). Type A garnets – characterized by high Mg and low Ca contents – are attributed to high-grade granulite-facies metasediments, charnockites and intermediate–acidic igneous rocks. Type B garnets are generally affiliated with amphibolite-facies metasediments. However, if garnet compositions plot exclusively in the Bi subfield (spessartine-rich), a derivation from intermediate–acidic igneous rocks is suggested. High-grade metabasic (Type Ci) and ultramafic rocks (pyroxenite, peridotite/Type Cii) usually host the Mg-rich and Ca-rich Type C garnets. Garnets with high to very high Ca contents (Type D) are attributed to metasomatic rocks (skarn), very low-grade metabasic rocks and ultra-high temperature calc-silicate granulites (Mange and Morton 2007).

The ternary diagrams Alm–Prp–Grs and Alm–Prp–Sps of Méres (2008) and Aubrecht et al. (2009) distinguish
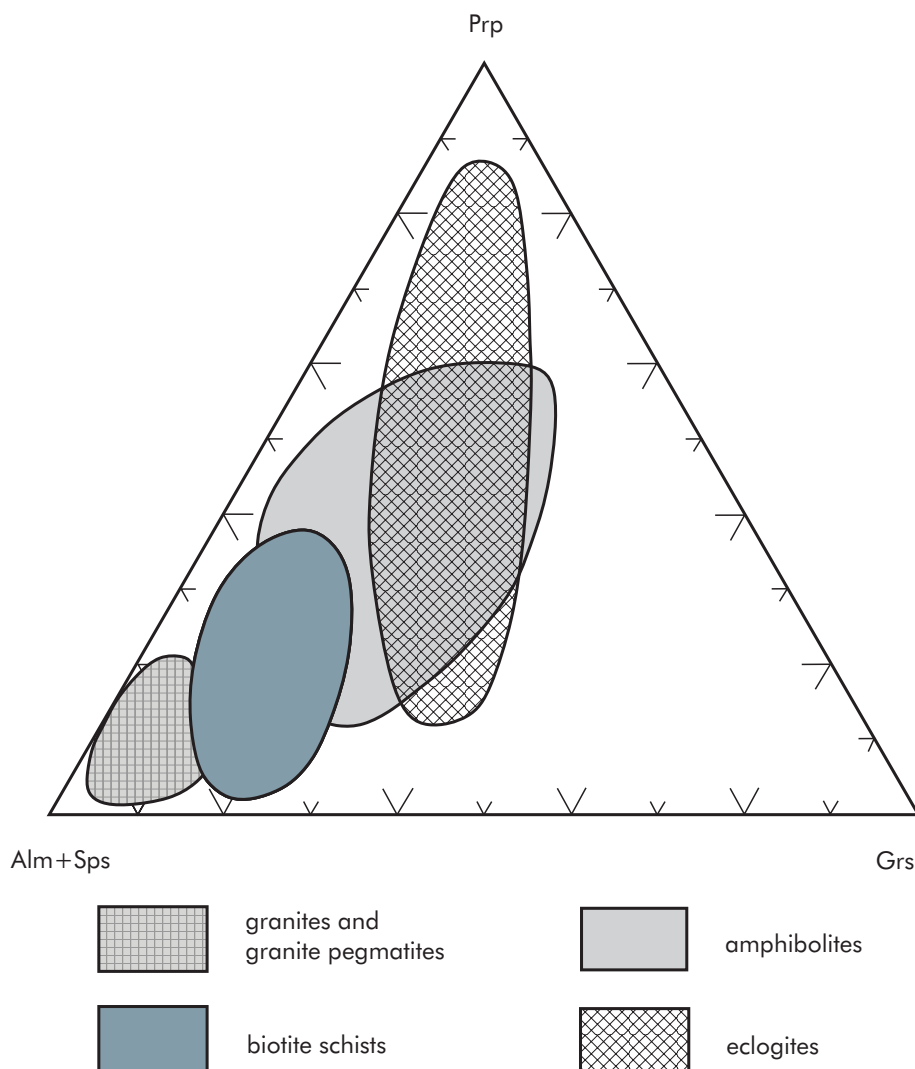

Fig. 1 Ternary garnet discrimination diagram (mol. %) with four subfields (granites and granite pegmatites, amphibolites, biotite schists and eclogites) modified after Preston et al. (2002).
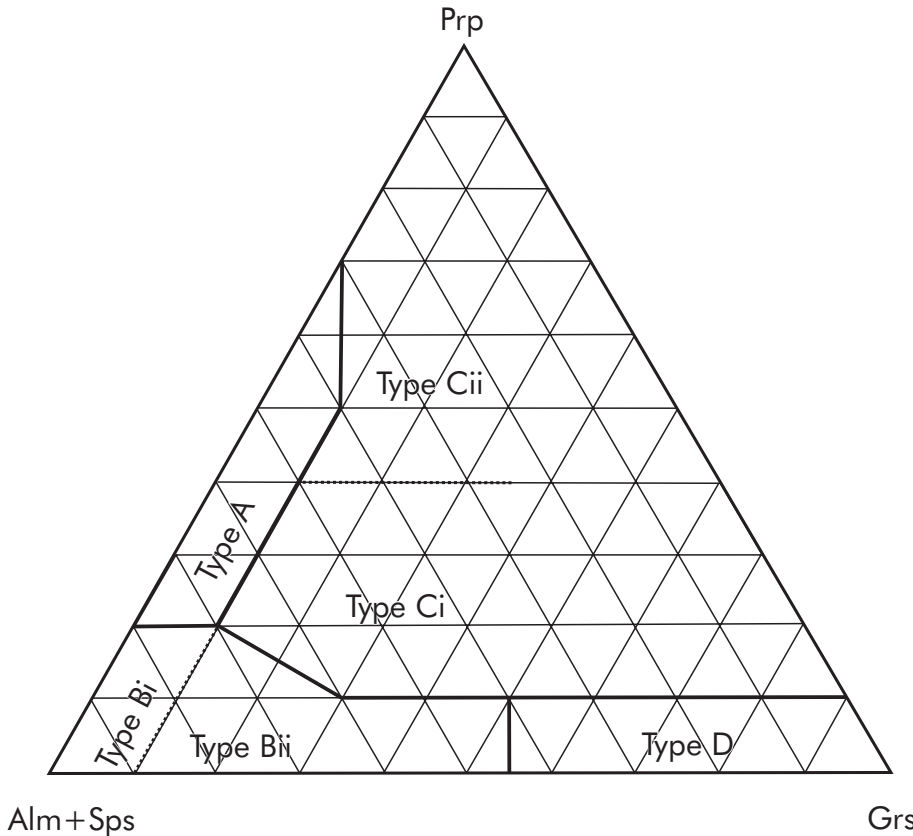
Fig. 2 Ternary garnet discrimination diagram (mol. %) with six subfields (see text for further details) modified after Mange and Morton (2007).

between seven groups of possible sources of metamorphic garnets (Fig. 3): (1) UHP eclogites or garnet peridotites, (2) HP eclogites and HP mafic granulites, (3) felsic and intermediate granulites, (4) gneisses metamorphosed under P–T conditions transitional between granulite- and amphibolite-facies, (5) amphibolites metamorphosed under P–T conditions transitional between granulite and amphibolite-facies, (6) amphibolite-facies gneisses and (7) amphibolites (s.s.). Based on the chemistry, garnets are thus generally divided into those (A) from high- to ultra-high pressure rocks, (B) from eclogite- and granulite-facies rocks, (C1) rocks crystallizing between granulite- and amphibolite-facies conditions and (C2) amphibolite-facies rocks.
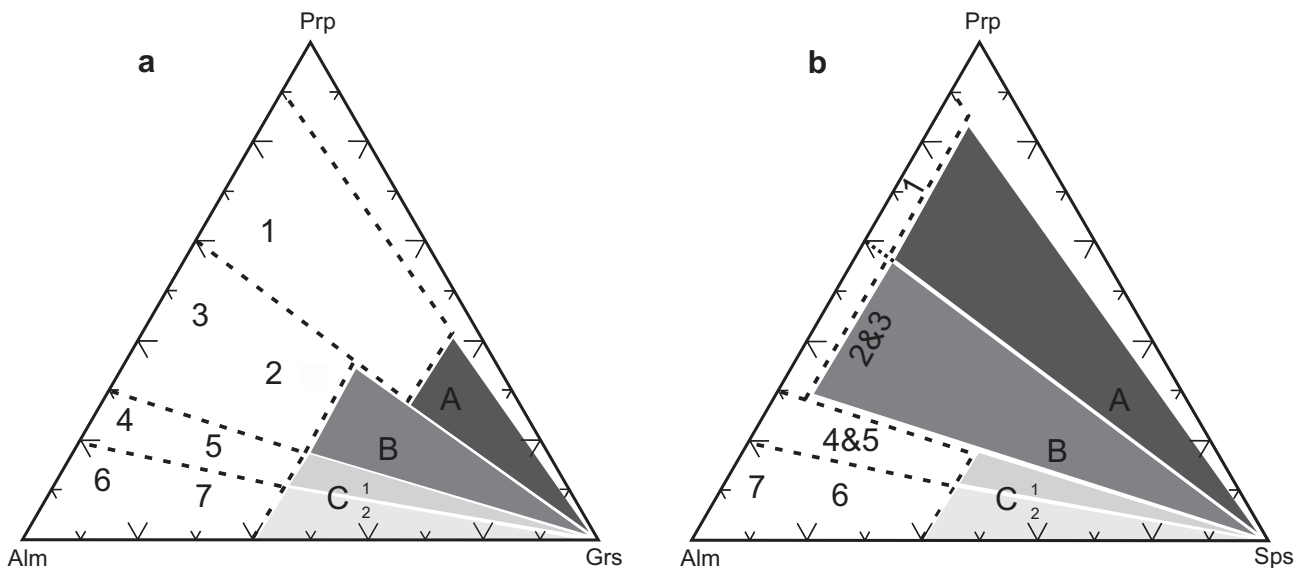

Fig. 3 Ternary garnet discrimination diagrams Alm–Prp–Grs (a) and Alm–Prp–Sps (b) (mol. %) with seven subfields (see text for further details). Modified from Méres (2008) and Aubrecht et al. (2009).

Suggate and Hall (2014) introduced an alternative discrimination diagram (Fig. 4) that also takes into account the end-members andradite and schorlomite. In order to discriminate garnets, they proposed a multi-stage method-
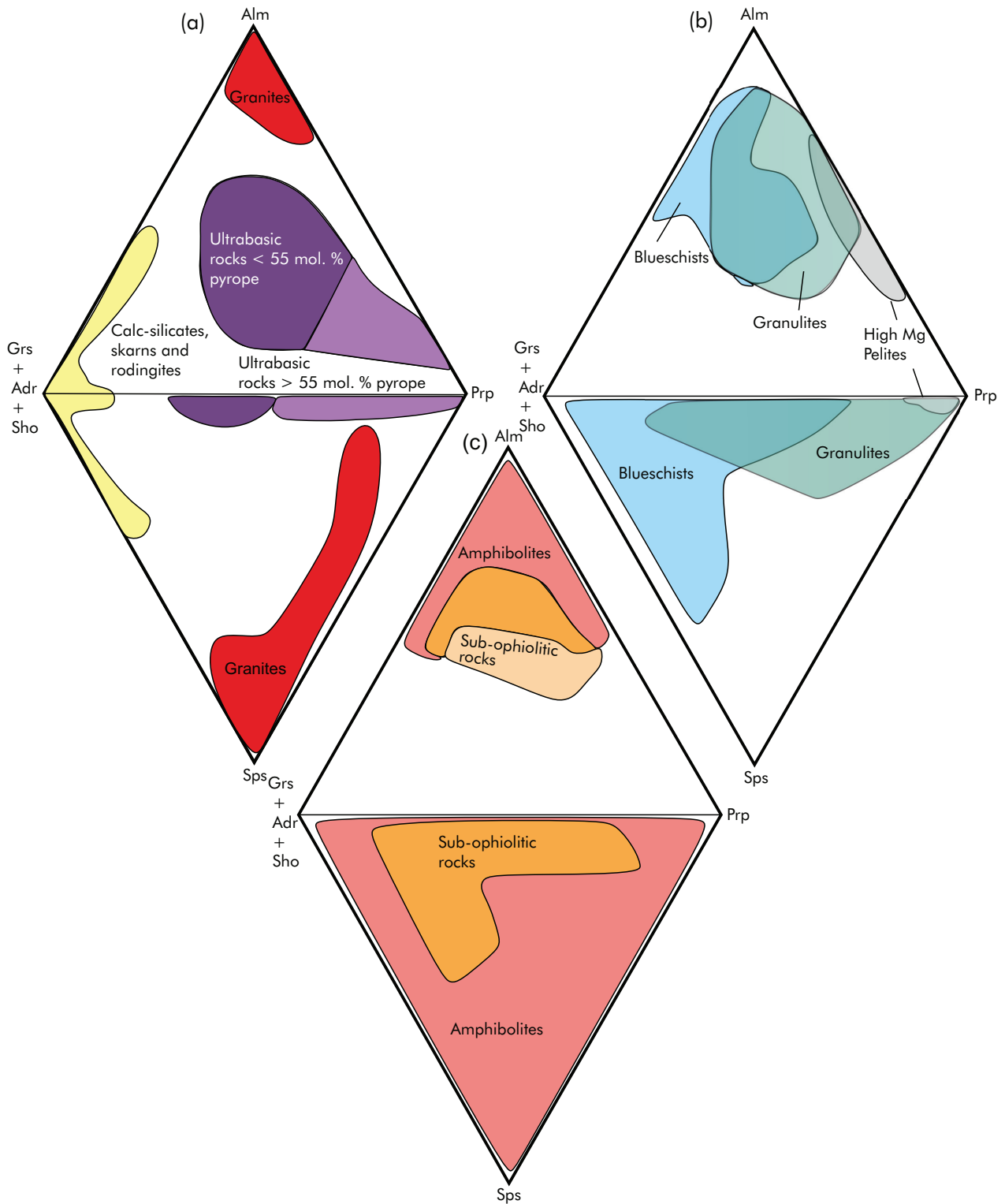

Fig. 4 Garnet provenance diagram of Suggate and Hall (2014) using double-ternary plots with the end-members grossular (Grs) + andradite (Adr) + schorlomite (Sho), almandine (Alm), pyrope (Prp) and spessartine (Sps) (mol. %).

ology, starting with the removal of garnets with unusual contents of Y_2O_3, V_2O_3 and ZrO_2, as well as the separation of garnets with high contents of TiO_2. In the next step, garnets with high contents of uvarovite and pyrope usually derived from ultramafic rocks are distinguished. Subsequently, the chemistry of the remaining garnets from specific metamorphic grades and the separated subgroups is visualized in two ternary plots with the vertices Alm, Prp, Sps, and Grs + And + Sho.

Tolosano-Delgado et al. (2018) recently published a multivariate discrimination approach relying on linear discriminant analysis with cross-validation. Based on an extensive database (n = 3,188), the approach enables a quantitative classification of garnets into five major host groups (eclogite-facies rocks, amphibolite-facies rocks, granulite-facies rocks, ultramafic rocks and igneous rocks).

Detailed analyses of trace elements in garnets were also shown to be useful for discriminating source rocks (e.g., Fedorowich et al. 1995; Otamendi et al. 2002; Čopjaková et al. 2005; Jung and Hellebrandt 2006; Krippner et al. 2014; Jedlička et al. 2015). In addition to elemental analyses, the metamorphic grade of garnets can be roughly assessed by investigating grain inclusions (Krogh 1982; Wendt et al. 1993; Méres et al. 2012; Schönig et al. 2018).

2.4. Limitations of conventional ternary garnet discrimination diagrams

The accuracy of representing chemical compositions of garnets that are commonly dominated by the four end-members almandine, grossular, pyrope and spessartine in ternary diagrams is limited. Krippner et al. (2014) highlighted a high degree of inaccuracy regarding particular classification subfields in the discrimination diagrams of Preston et al. (2002), Mange and Morton (2007), Méres (2008) and Aubrecht et al. (2009). The success rate for an unambiguous classification of certain garnet groups (e.g., amphibolite-facies metasedimentary garnets) in ternary diagrams is relatively low (Krippner et al. 2014). Moreover, the origin of garnets that are dominated by other end-members such as andradite, uvarovite or schorlomite cannot be inferred from these ternary discrimination diagrams.

In the case of the discrimination diagrams of Preston et al. (2002) and Mange and Morton (2007), the end-members spessartine and almandine are attributed to one vertex in each diagram. This is particularly relevant for discrimination between specific spessartine-rich metasedimentary garnets and garnets of intermediate–felsic igneous rocks (granodiorites, granites and pegmatites). As indicated by the classification diagrams of Preston et al. (2002) and Mange and Morton

(2007), average garnets of granodiorites, granites and pegmatites exhibit higher spessartine contents than metasedimentary garnets (Deer et al. 1982; Manning 1983). However, since garnets of greenschist-facies, lower blueschist-facies and lower amphibolite-facies rocks also tend to show elevated spessartine contents, an accurate interpretation of the chemistry of garnets in terms of their origin is hampered (Deer et al. 1982; Suggate and Hall 2014). Poor discrimination potential regarding the distinction of spessartine-rich metasedimentary amphibolites (biotite schists) and spessartine-rich intermediate–felsic igneous rocks (granites and granite pegmatites) in the diagrams of Preston et al. (2002) and Mange and Morton (2007) is obvious (Krippner et al. 2014). The discrimination diagrams for metamorphic garnets of Méres (2008) and Aubrecht et al. (2009) do not combine two end-members at a certain vertex, but rather are merely based on the three end-member systems Alm–Prp–Grs and Alm–Prp–Sps. Hence, discrimination of calc-silicate (metasomatic) and intermediate–felsic igneous rocks is not possible.

The double-ternary discrimination diagrams of Suggate and Hall (2014) are especially useful alternative tools for deciphering the provenance of garnets with rather unusual compositions since this approach also considers andradite and rare schorlomite end-members. However, these diagrams also do not fully resolve the problem of overlaps between garnets of amphibolites, granulites, blueschists and eclogite-facies rocks (Krippner et al. 2014).

3. Materials and methods

3.1. Samples

Lower Miocene, garnet-rich sediment samples of the Fels Fm. (S1) and the Laa Fm. (S2) were collected in the Lower Austrian Molasse Basin, at *Fels am Wagram* (48°27'39.82"N, 15°48'42.09"E) and *Kirchberg am Wagram* (48°26'21.10"N, 15°51'7.35"E) and in the Upper Austrian Molasse Basin at *Gurten* (48°14'57.99"N, 13°20'42.31"E) (Fig. 5). Sediments of the Fels Fm. are characterized by well-sorted, fossil-rich medium and coarse sands. The Laa Fm. comprises yellowish brown, mica-rich medium and fine sands. For more detailed information on the sedimentological characteristics of both formations, see Roetzel et al. (1999) and Roetzel (2016). The Upper Austrian Oncophora Fm. comprises brownish-grey, diffusely layered clayish silts and light brown, mica-rich fine sands with intercalated pelitic layers. For additional information on the sedimentological characteristics of the Oncophora Fm. see Rupp et al. (2011).
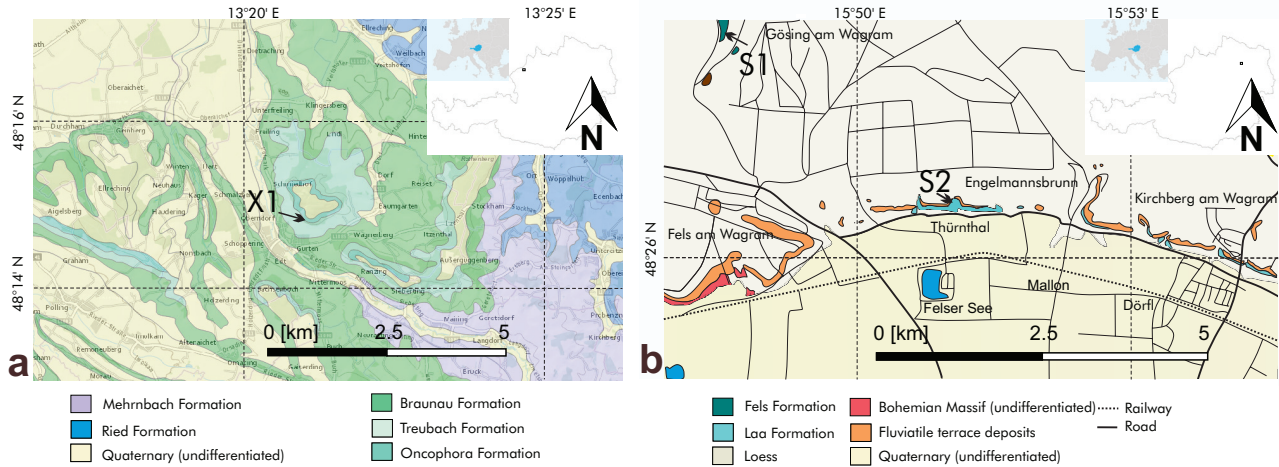
Fig. 5 Geological maps with sample locations. **a** – Sample location X1 (Upper Miocene Oncophora Fm.) in Upper Austria with other Miocene deposits (Ried, Mehrnbach, Treubach and Braunau formations). **b** – Sample locations S1 (Lower Miocene Fels Fm.) and S2 (Middle Miocene Laa Fm.) in Lower Austria.

3.2. Heavy-mineral analyses

The collected samples were treated with 40% acetic acid $(C_2H_4O_2)$ for five days to remove carbonate material. After drying in an oven, heavy minerals of the 0.063–0.4 mm sieve fraction were separated using the tetrabromethane heavy liquid (density 2.97 g/cm³). Heavy-minerals (n minimum = 200) were identified under a Nikon Type 104 polarized light microscope (Nikon Instruments Europe BV, Amsterdam, Netherlands).

3.3. Electron-probe microanalysis

For electron-microprobe analyses, heavy minerals were embedded in one-inch epoxy mounts (Araldite) and subsequently polished and carbon-coated. Garnet analyses were performed at the Department of Lithospheric Research by means of a Cameca SX100 electron-probe microanalyzer (EPMA) equipped with four wavelength spectrometers (WDS) and one energy-dispersive spectrometer (EDS). Well-characterized homogeneous natural and synthetic minerals were used as standards. All garnet analyses were carried out using a focused beam at 15 kV accelerating voltage and 20 nA beam current.

The counting time was 20 s at the peak position and 10 s at each background position.

For matrix correction, the PAP method (Pouchou and Pichoir 1991) was applied to all acquired data (Si, Al, Fe, Ca, Cr, Mg, Mn and Ti). The relative errors of the internal laboratory standard were below 1 % (Fig. 6). Garnet formulae were recalculated on the basis of 12 oxygen atoms and end-member proportions obtained using a Microsoft Excel spreadsheet (Locock 2008).

4. Results

4.1. TETGAR_C

In order to overcome some limitations of conventional ternary garnet discrimination diagrams, a tetrahedral garnet discrimination plot and calculation tool (TETGAR_C) has been developed (Knierzinger et al. in print; see also Theune 2005; D'Errico 2012). TETGAR_C is an improved version of TETGAR (Knierzinger et al. in print) that is based on the four garnet end-members (in mol. %): almandine (Alm), grossular (Grs), pyrope (Prp) and spessartine (Sps). TETGAR_C was programmed using MATLAB (version 2016a).

The following Cartesian coordinates define the vertices of the regular tetrahedron.

$$Alm = \frac{1/1}{1} \; Grs = \frac{3/1}{1} \; Prp = \frac{2/2.732}{1} \; Sps = \frac{2/1.577}{2.633} \qquad (1)$$

Cartesian coordinates were recalculated from normalized end-member values.

The space coordinates of any given garnet composition in TETGAR_C are calculated as follows:

$$Alm(\%) + \frac{3/1}{1} Grs(\%) + \frac{2/2.732}{1} Prp(\%) + \frac{2/1.577}{2.633} Sps(\%) \quad (2)$$

Space coordinates of given garnet compositions are directly calculated by the MATLAB function that can be found online as supplementary data.

Integrated subfields in this tetrahedral discrimination plot are based on the chemistry of more than 2,600 garnet samples. A database of Suggate and Hall (2014) and additional electron-microprobe data (Brown 1969; Shimazki 1977; Okay 1980; Manning 1983; Mathavan
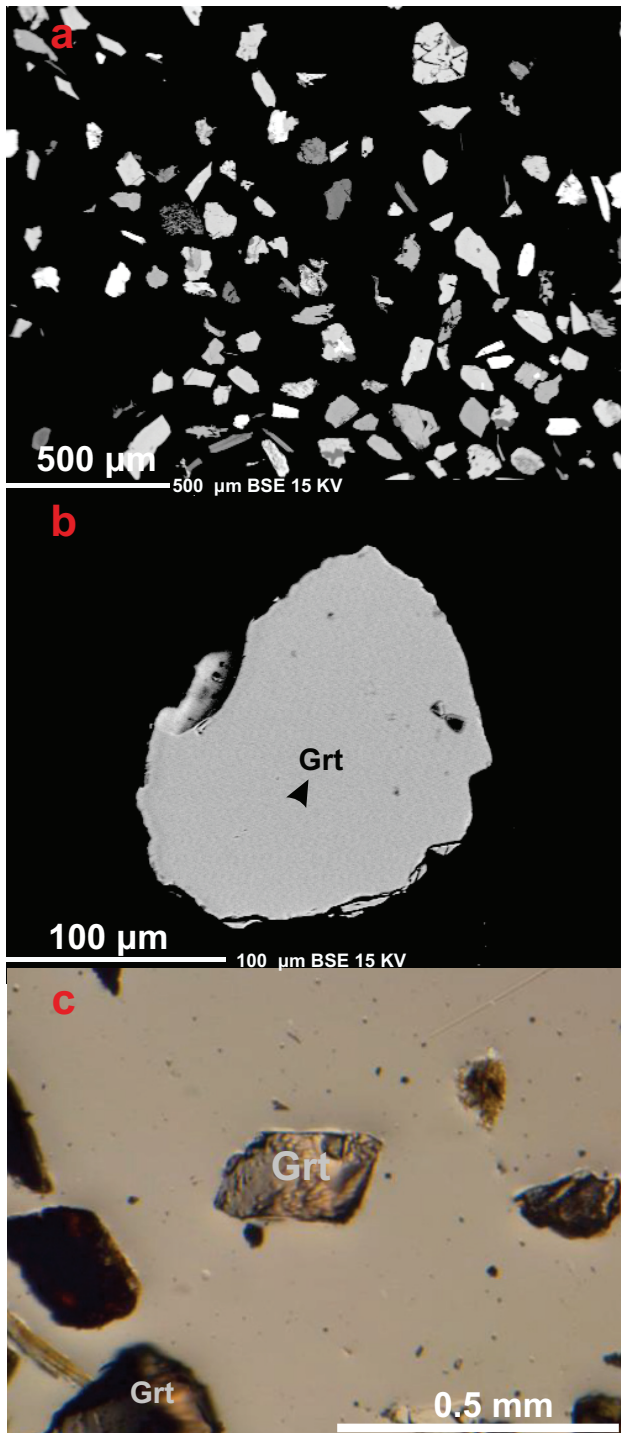
Fig. 6a Backscattered-electron images (BSE) of polished heavy minerals of the Laa Fm. **b** – Single garnet (Grt) grain of the Fels Fm. (BSE). The black arrow marks the location of WDS measurement of garnet mineral grain. **c** – Initial to advanced corrosion on surfaces of garnet grains of the Laa Fm. (centre). Plane-polarized light.

1989; Shenbao 1993; Klemd et al. 1994; Paulick and Franz 2001; Willner et al. 2001; Ballèvre et al. 2003; Dasgupta and Pal 2005; Drahota et al. 2005; Polyakova et al. 2005; Makrygina and Suvorova 2011; Malvoisin

et al. 2011; Antao 2013) are used as underlying data for the integrated subfields in TETGAR_C. The entire list of garnet compositions used for this study can be found as online supplementary material.

Based on the freely-accessible database of Suggate and Hall (2014) and additional EPMA data (see Introduction), various triangulated subfields representing mean chemical compositions of garnets of calc-silicate rocks, felsic igneous rocks (granites/pegmatites) and metasedimentary and metaigneous rocks of various metamorphic grades were integrated into TETGAR_C (Tab. 1). The data volume was compressed and only garnets in the range of ($\pm$) one standard deviation (σ) of the arithmetic mean (μ) for each end-member (Alm, Prp, Grs and Sps) were taken into account. Accordingly, each subfield represents ~68 % of all garnets considered for a specific subgroup (1σ confidence interval).

Garnets with higher other (e.g., andradite, uvarovite) end-member components ($\geq$ 4 %) were discarded. Garnets from rare ores, xenoliths, volcanic rocks, hornfelses, those with unclear or ambiguous attribution as well as redundant measurements were also disregarded. Due to their level of heterogeneity and insufficient data, migmatitic rocks were not explicitly considered either, although smooth transitions between rock types prevented a complete exclusion of migmatitic rock characteristics and hence an unambiguous attribution (see e.g., Gföhl Unit).

In order to calculate spatial coordinates of the plotting points in the tetrahedron, normalization of data to 100 % was performed (see supplementary data). The classification of garnets relies on a subdivision into ten garnet groups (Figs 7–10): (1) granites and pegmatites [pe][1], (2) greenschist-facies metasedimentary rocks [gre], (3) amphibolite-facies metasedimentary rocks [sedam], (4) amphibolite-facies metaigneous[2] rocks [metigam], (5) blueschist-facies metaigneous and metasedimentary rocks [blue], (6) calc-silicate rocks [cal], (7) granulite-facies metasedimentary rocks [sedgra], (8) granulite-facies metaigneous rocks [metiggra], (9) eclogite-facies metaigneous and metasedimentary rocks [ec] and (10) ultramafic rocks [maf].

The classification is partly based on Suggate and Hall (2014), Krippner et al. (2014) and Tolosano-Delgado et al. (2018) and does not comply with common rock classification schemes. It rather represents an attempt to establish a consistent nomenclature, enabling a reasonable comparison of garnet-bearing rocks.

The three-dimensional impression is ensured by using a colorbar (z-axis) that corresponds to the spessartine content. Integrated 3D-grid lines offer a better

---

[1] Abbreviation in TETGAR_C function.
[2] In this context, the term *metaigneous* comprises metabasic rocks and orthogneisses.
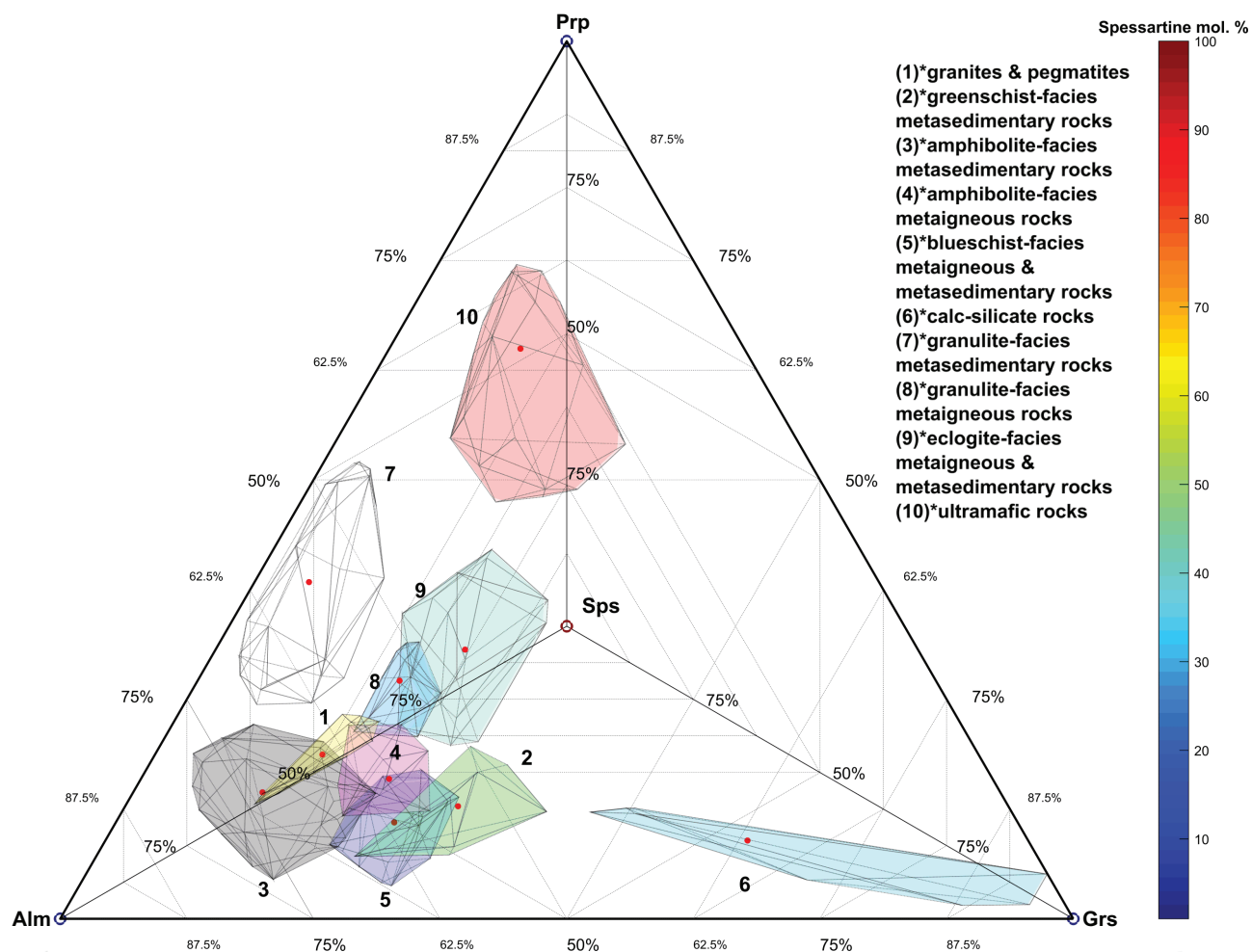
Fig. 7 TETGAR_C (top view) with integrated 3D-grid lines and ten subfields representing average garnet compositions of calc-silicate rocks, granites and pegmatites and different metamorphic facies of metasedimentary and metaigneous protoliths (mol. %). Red points denote mean values of the subfields.

spatial orientation and increase the general interpretation capacity of the plot. Dotted red lines denote the shortest distances to mean values of the subfields. If the user is familiar with the dimensions of the subfields, a single TETGAR_C figure (i.e., top view) is sufficient to identify the garnet suites with the highest correspondence.

In addition to the spatial information that can be extracted from TETGAR_C, the function directly calculates whether a certain point (single garnet measure-

Tab. 1 Selected garnets for triangulated subfields in TETGAR_C

Lithology	Chosen representative garnets (n)	Garnets within 1σ confindence interval	in %
Greenschist-facies metasedimentary rocks	41	14	34.14
Amphiboltie-facies metasedimentary rocks	279	126	45.16
Amphibolite-facies metaigneous rocks	42	17	40.47
Blueschist-facies metasedimentary & metaigneous rocks	149	75	50.33
Granulite-facies metasedimentary rocks	179	77	43.01
Granulite-facies metaigneous rocks	66	27	40.90
Eclogite-facies metasedimentary & metaigneous rocks	97	42	43.30
Granites & pegmatites	70	21	30.00
Ultramafic rocks	192	104	54.10
Calc-silicate rocks	37	11	29.72

Garnets within ±1σ of the arithmetic mean were used as underlying data for the triangulations
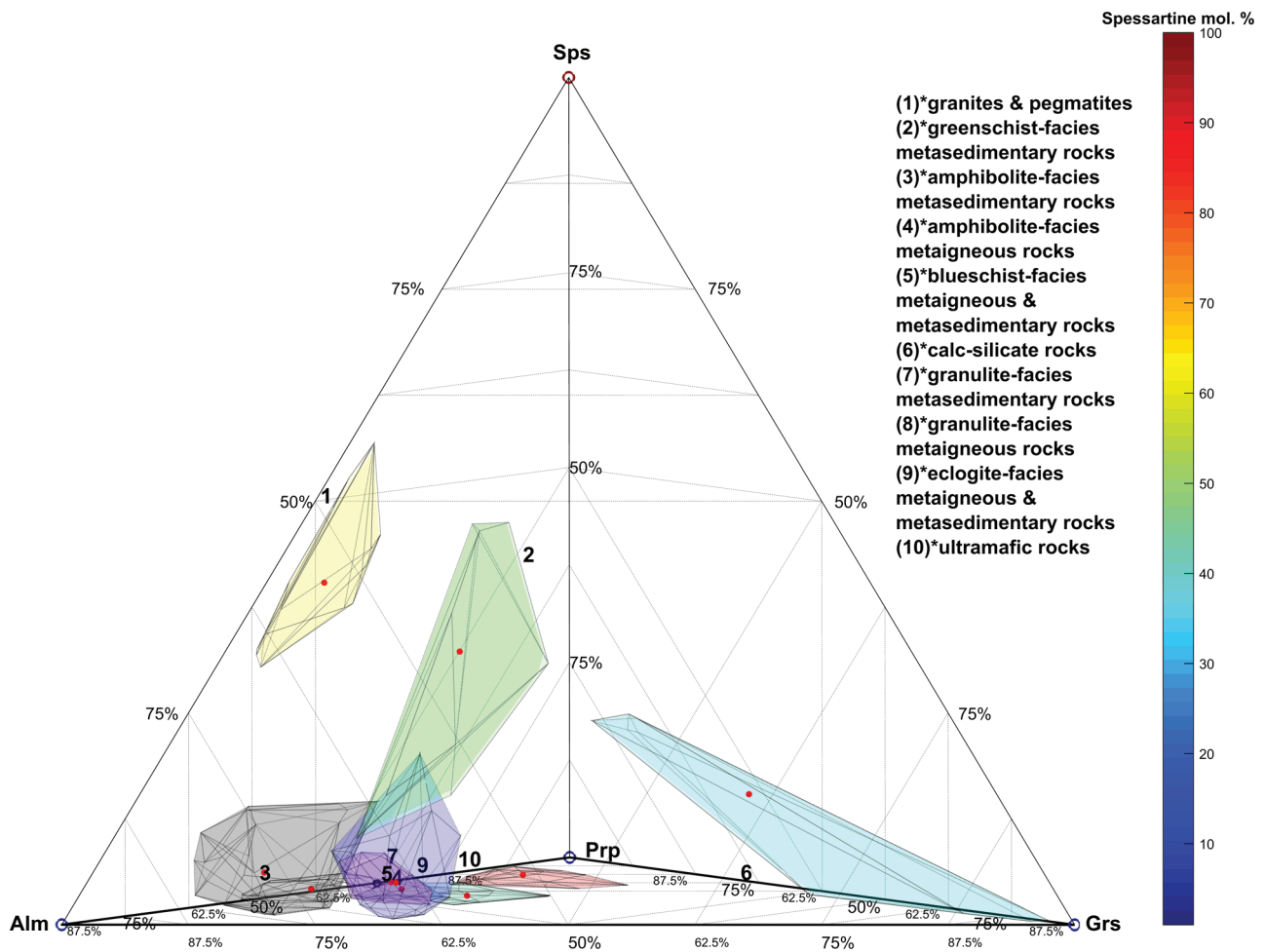
Fig. 8 TETGAR_C (front view).

ment) falls within a subfield or not. If a point is located within a subfield, it is plotted as a circle. If a point plots outside a subfield, it is displayed as a perforated flower structure. Moreover, TETGAR_C calculates the distance to the closest subfield mean value enabling an attribution to formation conditions and source rocks. Quantitative results are displayed in the MATLAB Command window.

4.2. Heavy-mineral analyses

The heavy-mineral assemblage of the Laa Fm. is characterized by a predominance of garnet (72 vol. %) and moderate to low concentrations of Ca-amphiboles (6.7 vol. %), epidote-group minerals (6.1 vol. %), aluminosilicate minerals (3.5 vol. %) and rutile (2.9 vol. %) (Fig. 11). Garnets of the Laa Fm. are colourless or pink and are primarily represented by subangular to subrounded grains, sometimes showing advanced degrees

of corrosion (see also Andò et al. 2012). The heavy-mineral spectrum of the Oncophora Fm. shows significantly higher amounts of epidote-group minerals (68.3 vol. %), smaller amounts of garnet (7.5 vol. %), rutile (7.0 vol. %), aluminosilicate minerals (5.1 vol. %), zircon (2.3 vol. %) and the Na-amphibole glaucophane (3.7 vol. %). Garnets in these sediments are relatively small (<100 μm). They are colourless or slightly pinkish, showing subangular to subrounded forms and initial to advanced corrosion states. The heavy-mineral assemblage of the Fels Fm. is dominated by garnet (43.6 vol. %) and staurolite (20.3 vol. %). Besides, lower amounts of epidote-group minerals (5.5 vol. %), tourmaline (4.3 vol. %), zircon (6.4 vol. %), rutile (5.5 vol. %), and aluminosilicate minerals (2.6 vol. %) are present. Garnets of the Fels Fm., mostly slightly pinkish with initial corrosion features, predominantly appear in angular to subangular form.
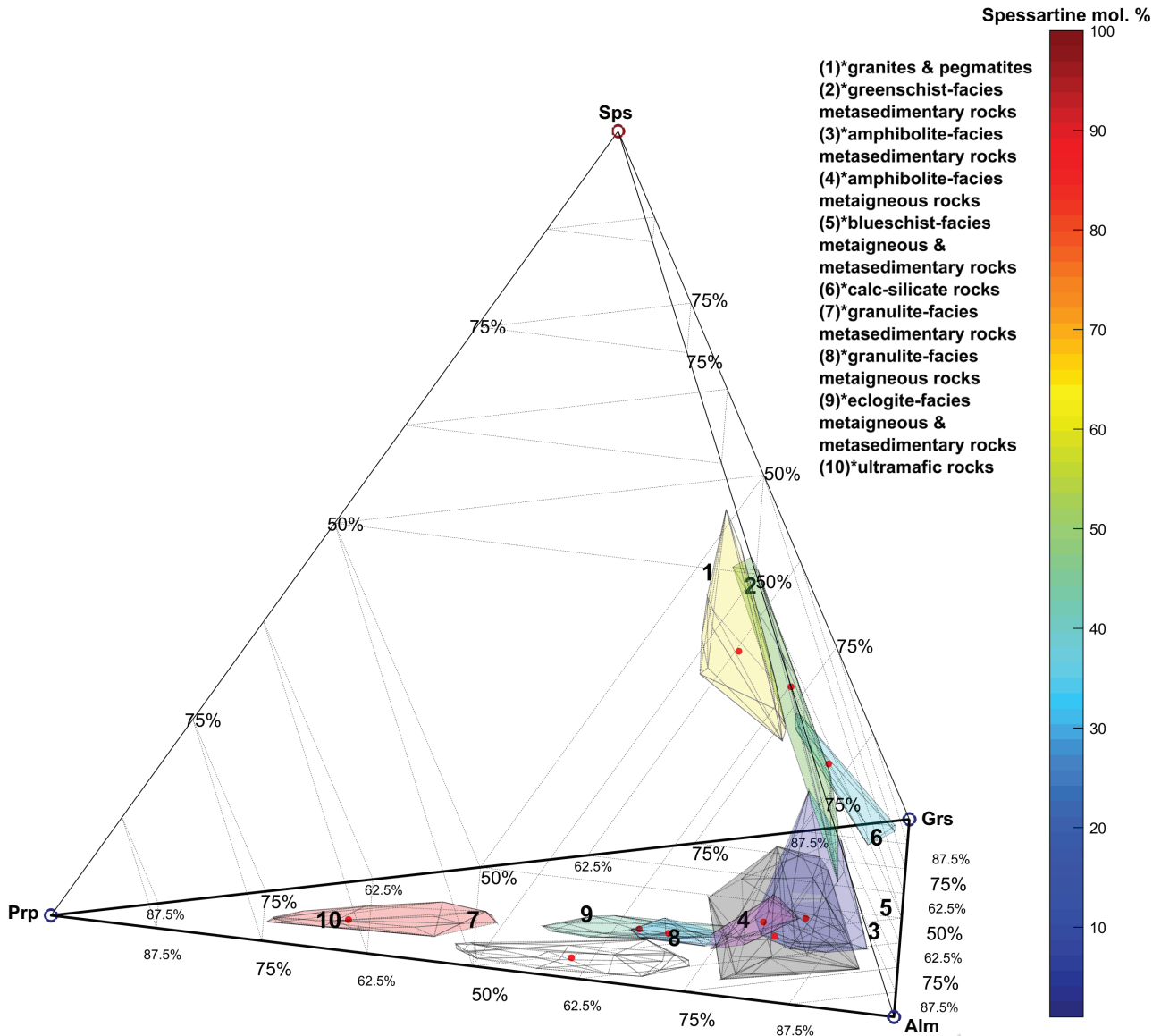
Fig. 9 TETGAR_C (side view).

5. Discussion

5.1. Case study of garnet provenance analysis using TETGAR_C

Heavy-mineral assemblages and chemical data from detrital garnets of the North Alpine Foreland Basin in both Lower Austria (Miocene; Laa Fm.; Fels Fm.) and in Upper Austria (Miocene; Oncophora Fm.) were used to evaluate TETGAR_C with respect to its potential to attribute almandine-rich garnets to their likely source rocks (Tab. 2).

Sediments are subject to constant alteration involving weathering processes, intrastratal dissolution and secondary mineral formation. Accordingly, (heavy) mineral assemblages of sedimentary deposits do not fully reflect the mineral composition of the source rocks and must, therefore, be interpreted with caution (Weltje and von Eynatten 2004; Andò et al. 2012).

Very high contents of epidote-group minerals (68.3%) in combination with considerable amounts of the high-pressure amphibole glaucophane in the Upper Austrian Oncophora Fm. are considered to be a strong indication of a predominant Alpine influence (see also von Eynatten et al. 1996; Garzanti et al. 2007; Neubauer et al. 2007; von Eynatten and Dunkl 2012; Krippner et al. 2015). This interpretation is backed up by a strong prevalence of the finest heavy-mineral fraction (<100 μm). Higher contents of epidote-group minerals and Ca-amphiboles in combination with a predominance
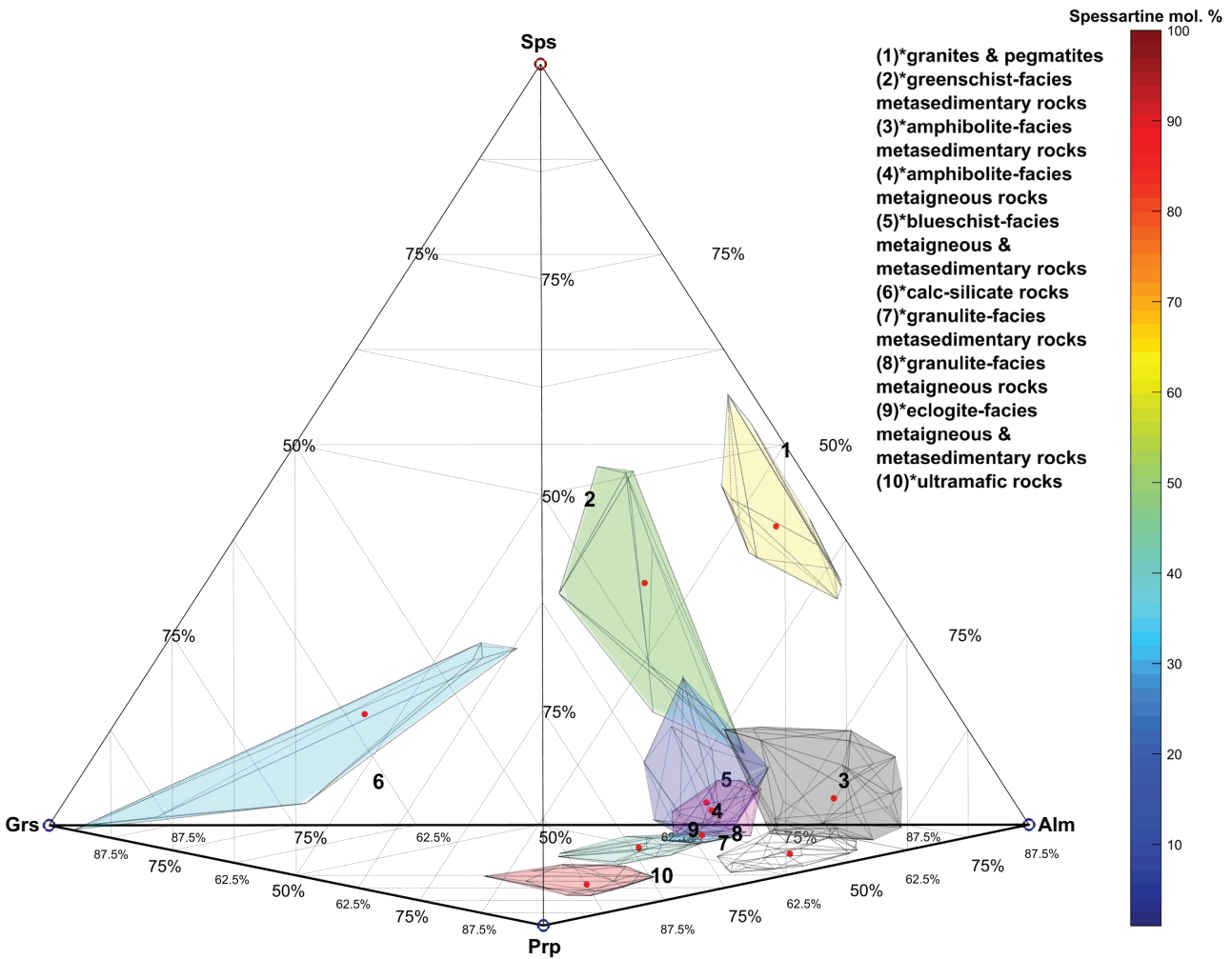
(1)*granites & pegmatites
(2)*greenschist-facies metasedimentary rocks
(3)*amphibolite-facies metasedimentary rocks
(4)*amphibolite-facies metaigneous rocks
(5)*blueschist-facies metaigneous & metasedimentary rocks
(6)*calc-silicate rocks
(7)*granulite-facies metasedimentary rocks
(8)*granulite-facies metaigneous rocks
(9)*eclogite-facies metaigneous & metasedimentary rocks
(10)*ultramafic rocks

Fig. 10 TETGAR_C (back view).

of garnet in the Laa Fm. also indicate an influence of Alpine source rocks (Faupl et al. 1988; Hagedorn and Boenigk 2008). Considerable amounts of staurolite, initial corrosion states of specific garnets and generally mixed grain size fractions (<100 μm to >350 μm) point towards an additional source in the surrounding area (Bohemian Massif). Unweathered to initial corrosion states of heavy minerals of the Fels Fm., characterized by high amounts of garnets and staurolite and relatively coarse grain sizes (Ø > 200 μm), suggest a predominant

local source in the Moldanubian or Moravian zones (see Fuchs and Matura 1976; Aliasgari 1993).

Notwithstanding possible implications from heavy-mineral analyses at this point, the depiction of the chemical compositions of garnets from the Laa and Fels formations by the discrimination diagram of Preston et al. (2002) suggests sources in granites and pegmatites on the one hand and biotite schists on the other (Fig. 12). Plotting data in the discrimination diagram of Mange and Morton (2007) implies an affiliation with metasedimentary amphibolites (Type B). However, since almost all garnets of the Fels Fm. are concentrated in the Bi subfield, an
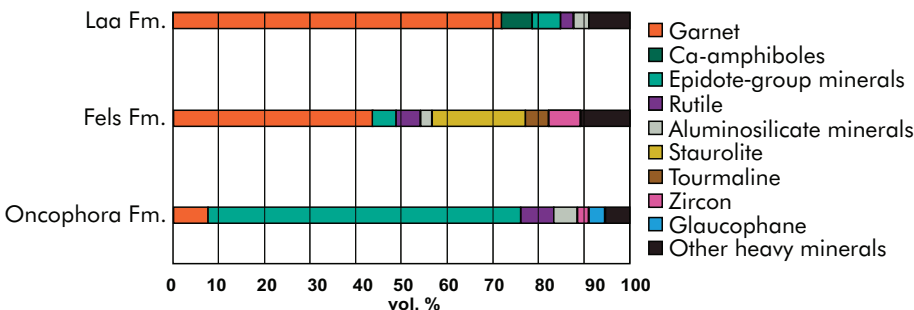

Fig. 11 Heavy-mineral assemblages of the Middle Miocene Laa Fm. (Lower Austria), the Middle Miocene Oncophora beds (Upper Austria) and the Lower Miocene Fels Fm. (Lower Austria). Presence of all explicitly mentioned minerals was verified by using EPMA.

Tab. 2 Representative garnet compositions of almandine garnets (in wt. %, atoms per formula unit and mol. %) of the Laa, Fels and Oncophora formations taken at the locations X1, S1 and S2.

Sample	Fels 1	Fels 2	Fels 3	Laa 1	Laa 2	Laa 3	Onc 1	Onc 2	Onc 3
SiO_2	36.974	37.116	37.409	37.383	36.919	37.315	37.169	37.096	37.093
TiO_2	0.080	0.063	0.020	0.089	0.237	0.095	0.092	0.089	0.182
Al_2O_3	20.887	20.994	21.307	21.390	21.199	21.438	21.482	21.652	21.275
Cr_2O_3	0.043	0.023	0.015	–	–	–	–	–	–
FeO	29.945	30.677	35.069	2.148	2.241	2.410	1.799	1.974	1.702
MnO	7.997	5.607	0.730	0.295	0.759	0.485	2.538	3.385	6.162
MgO	2.506	2.846	4.075	2.118	1.483	4.431	0.659	1.475	0.951
CaO	1.926	3.480	2.018	7.123	6.498	0.514	11.466	7.400	9.468
Total	100.406	100.807	100.629	100.743	100.499	100.414	100.374	100.686	100.665
Number of cations per formula unit (calculated on the basis of 12 oxygens)									
Si	2.986	2.973	2.979	2.976	2.966	2.976	2.965	2.961	2.964
Ti	0.005	0.004	0.001	0.005	0.014	0.006	0.006	0.005	0.011
Al	1.988	1.982	2.000	2.007	2.007	2.015	2.020	2.037	2.004
Cr	0.003	0.003	0.001	–	–	–	–	–	–
Fe^{2+}	2.022	2.055	2.335	2.148	2.241	2.410	1.799	1.974	1.702
Mn	0.547	0.380	0.049	0.020	0.052	0.033	0.171	0.229	0.417
Mg	0.302	0.340	0.484	0.251	0.178	0.527	0.078	0.176	0.113
Ca	0.167	0.299	0.172	0.608	0.559	0.044	0.980	0.633	0.811
Total	8.016	8.007	8.032	8.015	8.016	8.011	8.019	8.015	8.023
End-members (mol. %)									
Alm	66.6	66.9	76.8	71.0	74.0	80.0	59.4	65.6	55.9
Prp	9.9	11.1	15.9	8.3	5.9	17.5	2.6	5.8	3.7
Grs	5.5	9.7	5.7	20.1	18.5	1.5	32.4	21.0	26.6
Sps	18.0	12.4	1.6	0.7	1.7	1.1	5.7	7.6	13.7
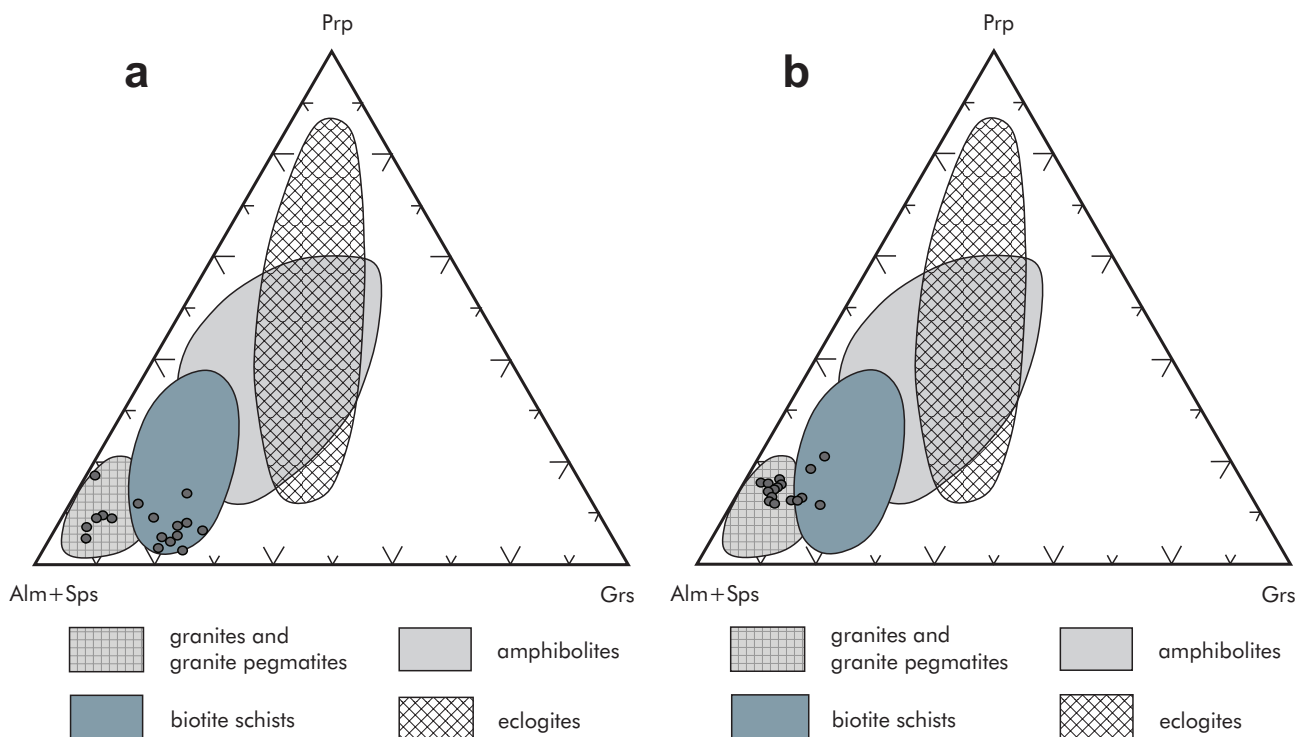
Fig. 12 Garnets of Laa (**a**) and Fels (**b**) formations in to the garnet discrimination ternary plot of Preston et al. (2002). For the Laa Fm. the diagram implies sources in 'granites and granite pegmatites' and 'biotite schists'. Garnets of the Fels Fm. are mainly associated with 'granites and granite pegmatites.
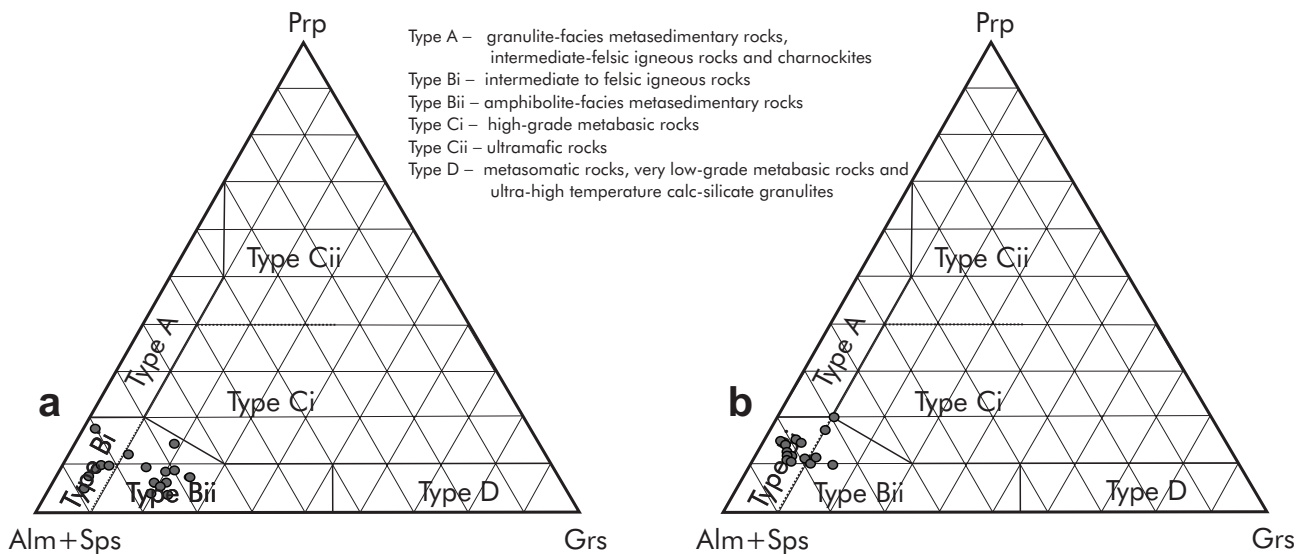
Fig. 13 Garnets of Laa (a) and Fels (b) formations in the garnet discrimination ternary plot of Mange and Morton (2007). For both formations, the diagram implies sources in 'amphibolite-facies metasedimentary rocks' and 'intermediate to felsic igneous rocks'.

origin in intermediate–felsic igneous rocks might also be considered (depending on sample size; Fig. 13).

Projection of the chemistry of the same garnets (Laa and Fels formations) in discrimination diagrams of Méres (2008) and Aubrecht et al. (2009) implies an attribution to amphibolite-facies gneisses (6) and amphibolites (s.s.) (7). Regarding provenance interpretation of garnets analyzed in this study, no strong concordance between the Alm–Prp–Grs diagram and the Alm–Prp–Sps diagram of Méres (2008) and Aubrecht et al. (2009) was achieved (Figs 14–15).

According to TETGAR_C, 33.3 % (6 out of 18) garnets of the Fels Fm. directly plot within the 1σ amphibolite-facies metasedimentary rock subfield. Calculating the

closest distance to subfield mean values for each plotting point suggests that all 18 garnets (100 % *sedam*; see function TETGAR_C) can be attributed to amphibolite-facies metasedimentary rocks (Fig. 16). The majority of those low-grossular almandines (~Alm_{71} Grs_6 Prp_{13} Sps_{10}) were probably formed in the sillimanite stability field and are affiliated with metasedimentary rocks (garnet micaschists) of the Moldanubian and Moravian zones (see also Bernroider 1989). This is in agreement with the heavy-mineral spectrum of the Fels Fm. that is dominated by garnet and staurolite (see also Aliasgari 1993; Nehyba and Roetzel 2010). Four (22.2 %; n = 18) garnets of the Laa Fm. plot within the 1σ amphibolite-facies metasedimentary rock subfield of TETGAR_C. According to the
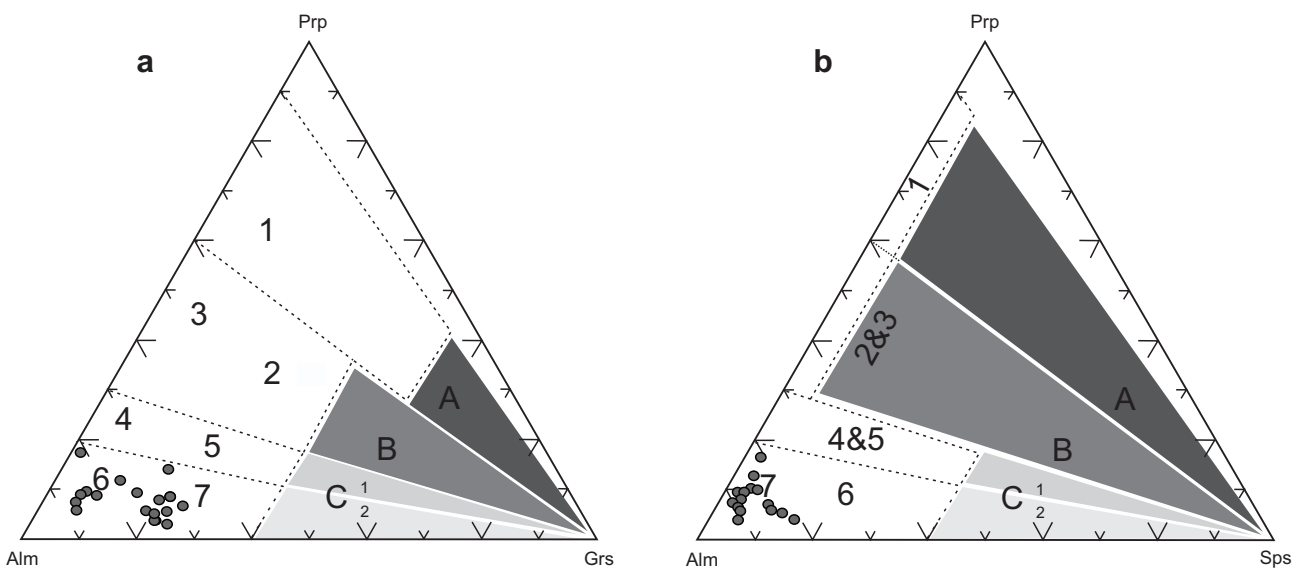

Fig. 14 Garnets of the Laa Fm. in the discrimination diagrams of Méres (2008) and Aubrecht et al. (2009) suggesting a source in amphibolite-facies gneisses and amphibolites (s.s).
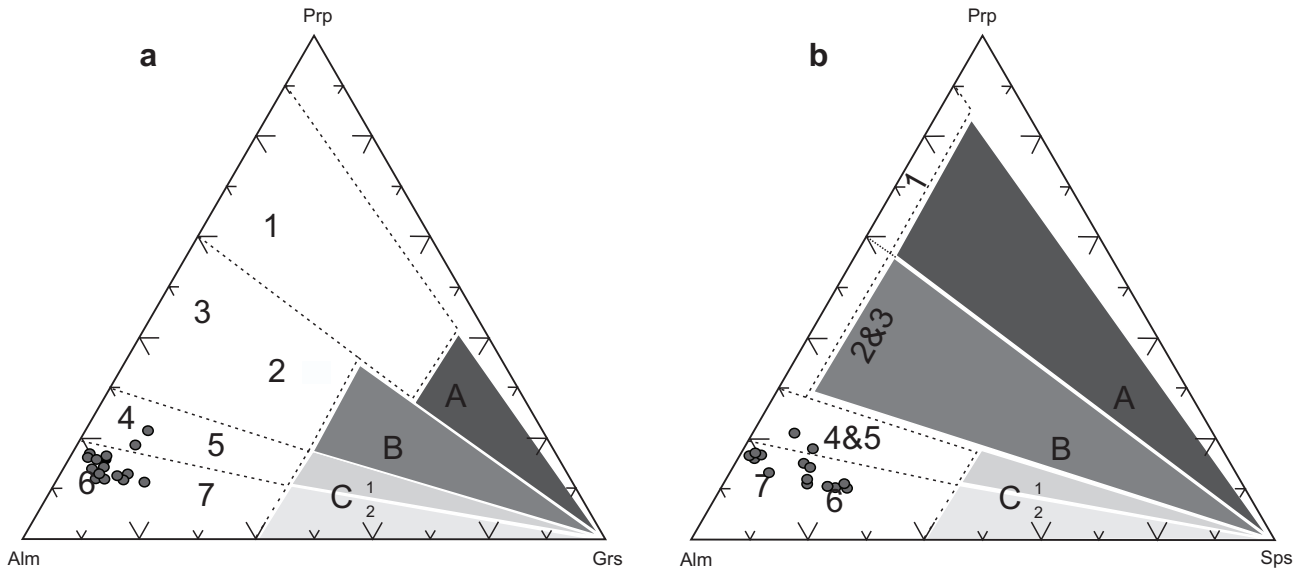
Fig. 15 Garnets of the Fels Fm. in the discrimination diagram of Méres (2008) and Aubrecht et al. (2009) suggesting a source in amphibolite-facies gneisses and amphibolites (s.s).
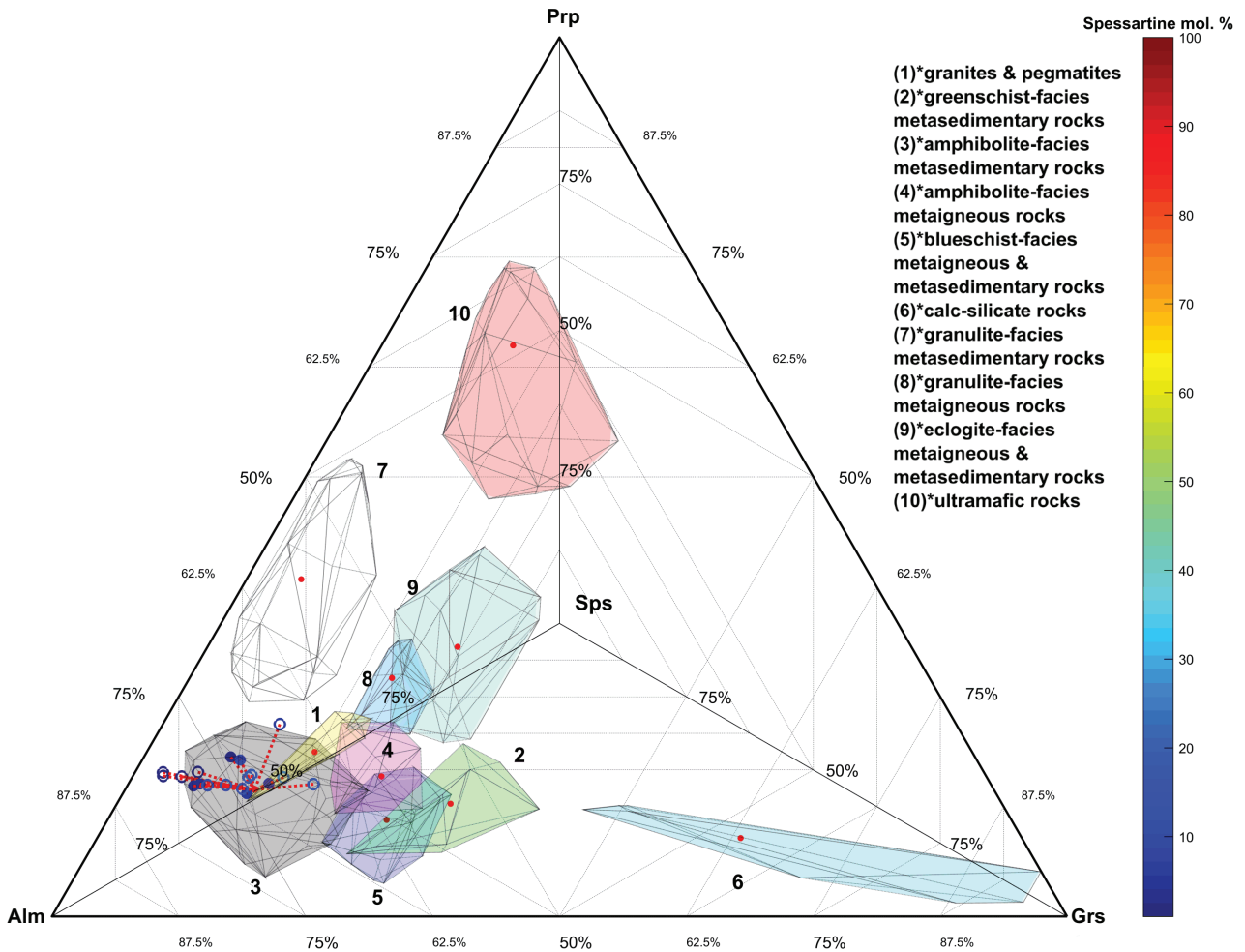

(1)*granites & pegmatites
(2)*greenschist-facies metasedimentary rocks
(3)*amphibolite-facies metasedimentary rocks
(4)*amphibolite-facies metaigneous rocks
(5)*blueschist-facies metaigneous & metasedimentary rocks
(6)*calc-silicate rocks
(7)*granulite-facies metasedimentary rocks
(8)*granulite-facies metaigneous rocks
(9)*eclogite-facies metaigneous & metasedimentary rocks
(10)*ultramafic rocks

Fig. 16 Garnets of the Fels Fm. plotted in TETGAR_C suggesting a main attribution (100%) to 'amphibolite-facies metasedimentary rocks' (TETGAR_C top view). The colormap corresponds to the spessartine content in mol. %. Red points are means of the individual subfields. Dotted red lines denote the shortest distances to the mean values of the subfields. Perforated flower structures symbolize garnet compositions that plot outside the ±σ subfields.
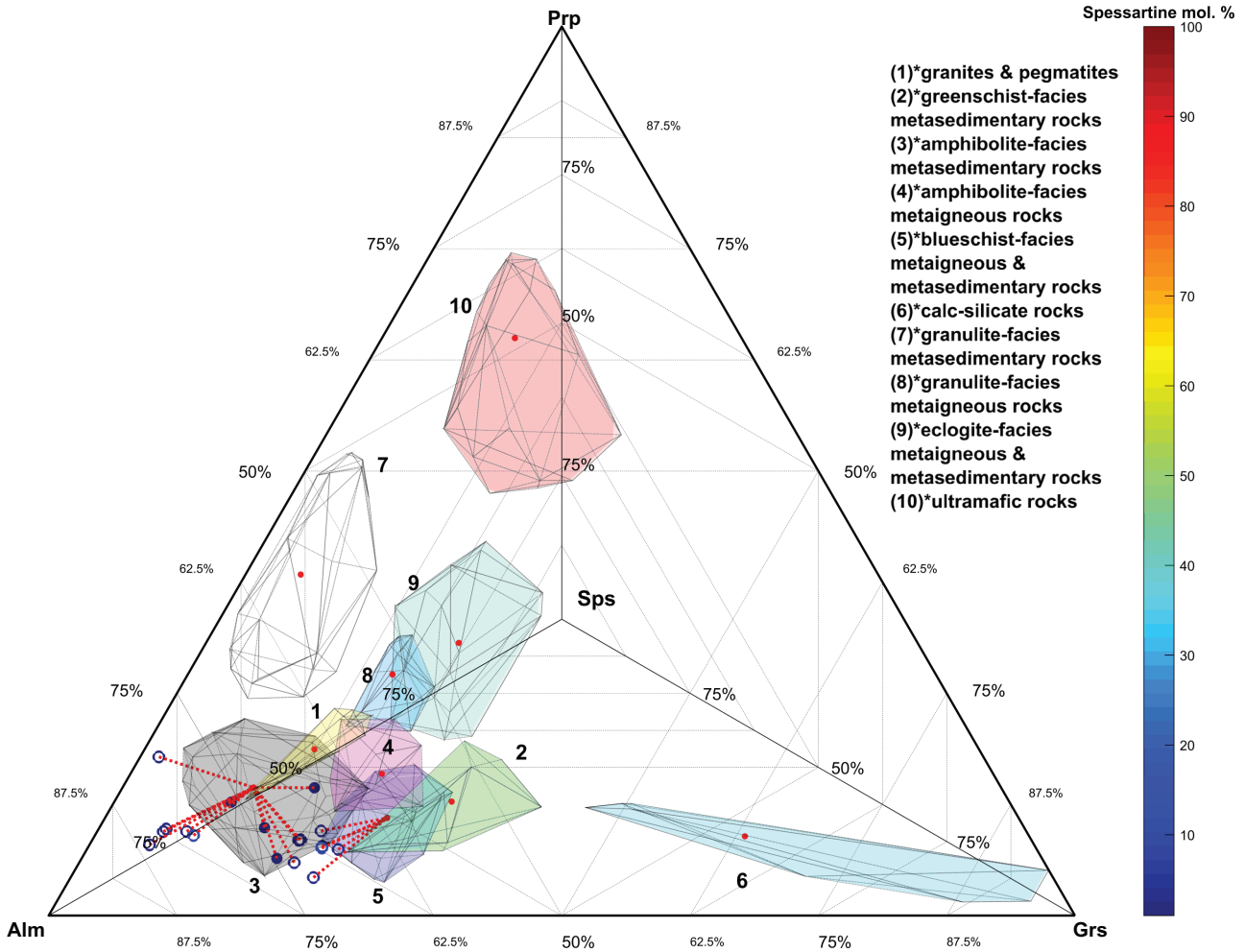
Fig. 17 Garnets of the Laa Fm. plotted in TETGAR_C suggesting a main attribution to 'amphibolite-facies metasedimentary rocks' (72.2%) and 'blueschist-facies metasedimentary & metaigneous rocks' (27.8%) (TETGAR_C top view).

integrated calculation feature, 13 garnets (72.2 %) are associated with amphibolite-facies metasedimentary rocks, and 5 garnets (27.8 %) with blueschists.

Grossular-rich almandines ($\sim Alm_{70} \, Grs_{20} \, Prp_7 \, Sps_3$) of the Laa Fm., situated in the transition zone between amphibolite-facies metasedimentary rocks and blueschists (Fig. 17), may have originated in the kyanite stability field in high-pressure metasedimentary rocks of the Alps (e.g., Bestel et al. 2009; Raič et al. 2012). Low-grossular almandines ($\sim Alm_{80} \, Grs_7 \, Prp_{10} \, Sps_3$) of the Laa Fm., in contrast, show affinity to metasedimentary rocks of the Moldanubian and Moravian zones.

The provenance interpretation of the Miocene Fels Fm. based on garnet discrimination approaches of Preston et al. (2002), Mange and Morton (2007), Méres (2008) and Aubrecht et al. (2009) is considered to be ambiguous or even erroneous. This is especially relevant concerning low-grossular almandines formed under amphibolite-facies conditions. For such low-grossular almandines

($\sim Alm_{80} \, Grs_5 \, Prp_{10} \, Sps_5$) the diagram of Preston et al. (2002) implies an association with felsic igneous rocks (granites and pegmatites). Plotting similar garnet compositions in the diagram of Mange and Morton (2007) also indicates intermediate–felsic source (Type Bi). The discrimination diagram of Méres (2008) and Aubrecht et al. (2009) principally does not allow an attribution to felsic igneous sources at all.

Interpreting the provenance of those low-grossular garnets of the Fels Fm. by TETGAR_C suggests exclusively amphibolite-facies metasedimentary sources. Based on the large and transparent underlying dataset of TETGAR_C, this conclusion is considered to be more accurate.

Low-grossular almandines are relatively common in sedimentary depositional systems, and better interpretability of this garnet group is deemed highly useful. There are arguably numerous disproportionate attributions of similar garnets to (intermediate–) felsic igne-

ous rocks in the literature (e.g., Krippner et al. 2015; Bassis et al. 2016; Nehyba and Opletal 2016; Hülscher et al. 2018).

5.2. Limitations of TETGAR_C

Because of the complex nature of metamorphic processes (e.g., composition of protolith; type of metamorphism), overlaps of discrimination subfields in TETGAR_C remain inevitable. Due to a lack of sufficient data, eclogite-facies rocks are not subdivided into metasedimentary and metaigneous rock associations in TETGAR_C. Since garnets usually do not occur in greenschist-facies metaigneous rocks, no such subfield was created either (Barker 1998).

Considerable overlap between amphibolite-facies metasedimentary and metaigneous rocks on the one hand and granulite-facies metaigneous and eclogite-facies rocks on the other is apparent but hardly avoidable due to similar garnet chemistries. Consideration of additional garnets associated with orthogneisses would probably lead to dimension changes of the metaigneous rock subfields (e.g., Povondra and Vrána 1996; Breiter et al. 2005; Chopin et al. 2012; Georgiadis et al. 2014).

Expansion of the underlying database and a consistent rock classification would certainly further increase the accuracy of the subfields (e.g., Tuccillo et al. 1990) and would presumably enable an integration of additional ones (e.g., charnockites, intermediate igneous rocks, hornfelses, orthogneisses, migmatites). A lack of statistical comparability is caused by considerable variability in the size of the corresponding datasets (calc-silicate rocks [n = 37]; metasedimentary rocks [n = 279]). Addition of further garnet analyses from calc-silicate rocks, greenschists (n = 41) and metaigneous amphibolites (n = 42) would be desirable.

Garnets of calc-silicate rocks are typically dominated by the grossular–andradite solid solution (e.g., Deer et al. 1982; Suggate and Hall 2014). For that reason, the grossular-rich calc-silicate rocks subfield in TETGAR_C represents only a particular group of garnets that are affiliated with calc-silicate rocks.

Following example deals with garnets of the Oncophora Fm. and highlights some ambiguities of TETGAR_C concerning provenance interpretation (Fig. 18). Although the integrated calculation feature of TETGAR_C implies a predominant attribution to blueschist-facies rocks, great care must be taken when interpreting the provenance, since the majority of garnets plot – similar to grossular-rich almandines of the Laa Fm. (see Fig. 17) – in the transition zone between greenschist-, amphibolite- and blueschist-facies rocks (Fig. 18).

According to TETGAR_C, seven garnets (70 %) are affiliated with blueschists, two (20 %) are linked to amphibolite-facies metasedimentary rocks and one might be attributed to amphibolite-facies metaigneous rocks.

Since the amphibolite-facies metasedimentary rocks subfield and the metasedimentary greenschist subfield are slightly more extended than the blueschist-facies subfield, the plotted points fall closer to the mean value of the blueschist-facies subfield. Taking this into account, a reliable affiliation with blueschists as dominant source rocks is debatable. One point in the transition zone between amphibolite-facies metasedimentary and blueschist-facies rocks plots in both subfields, further illustrating the limited discrimination efficiency of the subfields. An accurate affiliation is further complicated due to the small sample size (n = 10). However, for the Oncophora Fm., a considerable contribution of blueschist-facies garnets is also supported by the presence of the HP–LT mineral glaucophane.

5.3. Varying grossular contents in metasedimentary and metaigneous rocks

Representation of data in TETGAR_C suggests major compositional differences between garnets from metasedimentary and metaigneous rocks. In general, the former show lower grossular contents than the latter. Smaller differences between the two groups were noted with respect to blueschist-facies rocks.

Distinct grossular contents between metasedimentary and metaigneous rocks might be due to the relatively fast dissolution rate of Ca-rich feldspars in sedimentary environments.

Ca-rich feldspars (e.g., anorthite) are major constituents of igneous rocks, and they are also important reactants in the formation of grossular (Hufmann 2003). The dissolution rate of anorthite ($Ca[Al_2Si_2O_8]$) is very high (log rate: –8.55 mol/ m²/sec). The mean lifetime of a 1 mm anorthite crystal at 25 °C and pH 5 is about 112 yr (Lasaga 1984). By comparison, a quartz crystal (log rate: –13.39 mol/m²/s) of the same size and exposed to similar conditions has a mean lifetime of 34 Ma (Lasaga et al. 1994).

6. Conclusions

In comparison to other ternary garnet discrimination diagrams, the three-dimensional MATLAB-based TETGAR_C software enables a better spatial and quantitative differentiation of plotting points and hence a better interpretation of the origin of detrital garnets in many cases. The distinguished subfields are based upon a database of more than 2,600 garnets. The main function
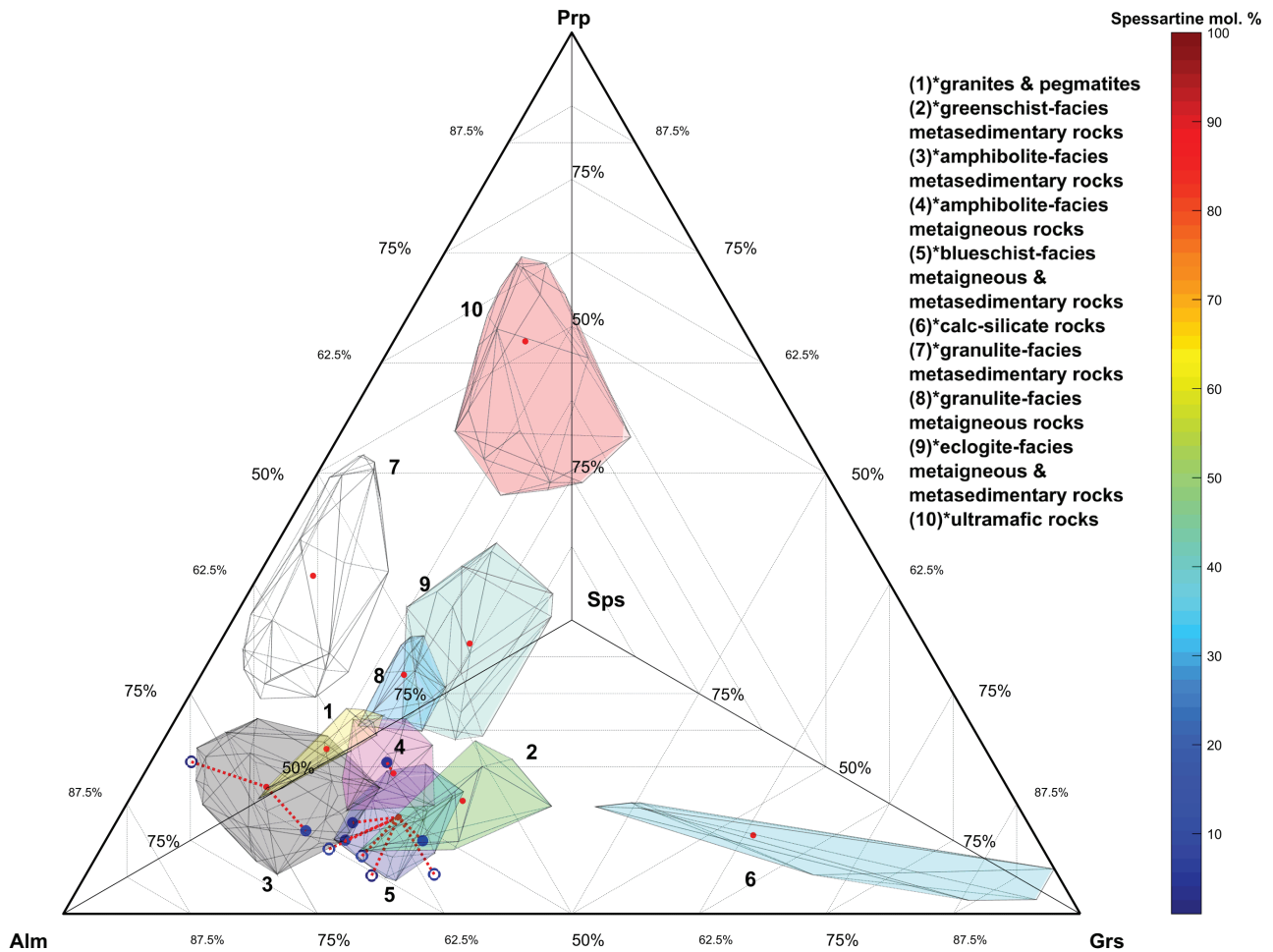
Fig. 18 Garnets of the Oncophora Fm. plot in the transition area between greenschists, blueschists and amphibolites. TETGAR_C (top view) indicates a primary attribution to 'blueschist-facies metaigneous & metasedimentary rocks' (70%) and 'metasedimentary amphibolites' (20%).

tests whether a point plots within a subfield and quantifies the distance to the closest mean value for any of the subfields.

Since conventional ternary discrimination diagrams combine or disregard certain end-member components, an unambiguous attribution to certain source rocks is hampered. Compared to these conventional ternary discrimination diagrams, the three-dimensional nature of the discrimination plot TETGAR_C reduces the overlaps among specific garnet subfields considerably. In particular, TETGAR_C enables a clearer distinction of the garnets from greenschist-facies, amphibolite-facies and blueschist-facies and felsic igneous rocks (granites and pegmatites) as well as a general differentiation between metaigneous and metasedimentary provenances from amphibolite- and granulite-facies rocks.

Although considerable differences between specific garnet groups in terms of data volume limit the statistical comparability of the subfields, the interpretation potential of TETGAR_C is considered to be superior to other ternary garnet discrimination diagrams with no specific underlying quantitative data.

Electronic supplementary material. Six tables, one video, a data input example (MS Word) and the MATLAB function (MS Word and M-file) are available at the Journal web site (*http://dx.doi.org/10.3190/jgeosci.284*).

References

ALIASGARI H (1993) Petrographische Untersuchungen an Glimmerschiefern im Bereich von Poigen, Fernitz und Langenlois (Moldanubikum). Jb Geol B–A 136: 19–25 (in German with English abstract)

ANDÒ S, GARZANTI E (2014) Raman spectroscopy in heavy-mineral studies. In: SCOTT RA, SMYTH HR, MORTON AC, RICHARDSON N (eds) Sediment Provenance Studies in Hydrocarbon Exploration and Production. Geological Society of London Special Publications 386, pp 395–412

ANDÒ S, BERSANI D, VIGNOLA P, GARZANTI E (2009) Raman spectroscopy as an effective tool for high-resolution heavy mineral analysis: examples from major Himalayan and Alpine fluvio-deltaic systems. Spectrochim Acta Part A 73: 450–455

ANDÒ S, GARZANTI E, PADOAN M, LIMONTA M (2012) Corrosion of heavy minerals during weathering and diagenesis: a catalog for optical analysis. Sediment Geol 280: 165–178

ANDÒ S, MORTON AC, GARZANTI E (2014) Metamorphic grade of source rocks revealed by chemical fingerprints of detrital amphibole and garnet. In: SCOTT RA, SMYTH HR, MORTON AC, RICHARDSON N (eds) Sediment Provenance Studies in Hydrocarbon Exploration and Production. Geological Society of London Special Publications 386, pp 351–371

ANTAO SM (2013) Is near-endmember birefringent grossular non-cubic? New evidence from synchrotron diffraction. Canad Mineral 51: 771–784

AUBRECHT R, MERES S, SYKORA M, MIKUS T (2009) Provenance of the detrital garnets and spinels from the Albian sediments of the Czorsztyn Unit (Pieniny Klippen Belt, Western Carpathians, Slovakia). Geol Carpath 60: 463–483

BALLÈVRE M, PITRA P, BOHN M (2003) Lawsonite growth in the epidote blueschists from the Ile de Groix (Armorican Massif, France): a potential geobarometer. J Metamorph Geol 21: 723–735

BARKER AJ (1998) Introduction to Metamorphic Textures and Microstructures. Psychology Press, Southampton, pp 1–290

BASSIS A, HINDERER M, MEINHOLD G (2016) New insights into the provenance of Saudi Arabian Palaeozoic sandstones from heavy mineral analysis and single-grain geochemistry. Sediment Geol 333: 100–114

BERNROIDER M (1989) Zur Petrogenese präkambrischer Metasedimente und cadomischer Magmatite im Moravikum. Jb Geol B–A 132: 349–373

BERSANI D, ANDÒ S, VIGNOLA P, MOLTIFIORI G, MARINO IG, LOTTICI PP, DIELLA V (2009) Micro-Raman spectroscopy as a routine tool for garnet analysis. Spectrochim Acta Part A 73: 484–491

BESTEL M, GAWRONSKI T, ABART R, RHEDE R (2009) Compositional zoning of garnet porphyroblasts from the polymetamorphic Wölz Complex, Eastern Alps. Mineral Petrol 97: 173–188

BOGGS S (2009) Petrology of Sedimentary Rocks. Cambridge University Press, Cambridge, pp 1–600

BREITER K, ČOPJAKOVÁ R, GABAŠOVÁ A, ŠKODA R (2005) Chemistry and mineralogy of orthogneisses in the northeastern part of the Moldanubicum. J Czech Geol Soc 50: 81–93

BROWN EH (1969) Some zoned garnets from the greenschist facies. Amer Miner 54: 1662–1676

CARACCIOLO L, ANDÒ S, VERMEESCH P, GARZANTI E, MCCABE R, BARBARANO M, PALEARI C, RITTNER M, PEARCE T (in print) A multidisciplinary approach for the quantitative provenance analysis of siltstone. Mesozoic Mandawa Basin, southeastern Tanzania. In: DOWEY P, OSBORNE M, VOLK H (eds) Application of Analytical Techniques to Petroleum Systems. Geological Society of London Special Publications 484, DOI: 10.1144/SP484-2018-136

CHOPIN F, SCHULMANN K, ŠTÍPSKÁ P, MARTELAT E, PITRA P, LEXA O, PETRI B (2012) Microstructural and metamorphic evolution of a high-pressure granitic orthogneiss during continental subduction (Orlica–Śnieżnik Dome, Bohemian Massif). J Metamorph Geol 30: 347–376

COOKE RA, O'BRIEN PJ, CARSWELL DA (2000) Garnet zoning and the identification of equilibrium mineral compositions in high-pressure–temperature granulites from the Moldanubian Zone, Austria. J Metamorph Geol 18: 551–569

ČOPJAKOVÁ R, SULOVSKÝ P, PATERSON BA (2005) Major and trace elements in pyrope–almandine garnets as sediment provenance indicators of the Lower Carboniferous Culm sediments, Drahany Uplands, Bohemian Massif. Lithos 82: 51–70

DASGUPTA S, PAL S (2005) Origin of grandite garnet in calc-silicate granulites: mineral fluid equilibria and petrogenetic grids. J Petrol 46: 1045–1076

DEER WA, HOWIE RA, ZUSSMAN J (1982) Rock-forming Minerals, Volume 1a, Orthosilicates. Halsted Press, New York, pp 1–936

DEER WA, HOWIE RA, ZUSSMAN J (1992) An Introduction to Rock-forming Minerals. Longman Group Ltd., Harlow, pp 1–712

D'ERRICO J (2012) Inhull. Accessed on April 1, 2019, at *https://de.mathworks.com/matlabcentral/fileexchange/10226-inhull?s_tid=mwa_osa_a*

DIETVORST EJL (1982) Retrograde garnet zoning at low water pressure in metapelitic rocks from Kemiö, SW Finland. Contrib Mineral Petrol 79: 37–45

Drahota P, Pertold Z, Pudilová M (2005) Three types of skarn in the northern part of the Moldanubian Zone, Bohemian Massif – implications for their origin. J Czech Geol Soc 50: 19–35

Faryad SW, Hoinkes G (2004) Complex growth textures in a polymetamorphic metabasite from the Kraubath Massif (Eastern Alps). J Petrol 45: 1441–1451

Faupl P, Rohrlich V, Roetzel R (1988) Provenance of the Ottnangian sands as revealed by statistical analysis of their heavy mineral content (Austrian Molasse Zone, Upper Austria and Salzburg). Jb Geol B–A 131: 11–20

Fedorowich JS, Jinesh CJ, Kerrich R (1995) Trace-element analysis of garnet by laser-ablation microprobe ICP–MS. Canad Mineral 33: 469–480

Fuchs G, Matura A (1976) Zur Geologie des Kristallins der südlichen Böhmischen Masse. Jb Geol B–A 119: 1–43 (in German with English abstract)

Garzanti E, Doglioni C, Vezzoli G, Andò S (2007) Orogenic belts and orogenic sediment provenance. J Geol 115: 315–334

Garzanti E, Resentini A, Andò S, Vezzoli G, Pereira A, Vermeesch P (2015) Physical controls on sand composition and relative durability of detrital minerals during ultra-long distance littoral and aeolian transport (Namibia and southern Angola). Sedimentology 62: 971–996

Georgiadis IK, Koroneos A, Papadopoulou L, Kantiranis N, Tamaropoulos AE, Tsirambides A (2014) Using detrital garnets to determine provenance: a case study from the Vertiskos Unit (Serbomacedonian Massif, N. Greece). Mineral Petrol 108: 187–206

Grew ES, Locock AJ, Mills SJ, Galuskina IO, Galuskin EV, Halenius U (2013) Nomenclature of the garnet supergroup. Amer Miner 98: 785–810

Grütter HS, Gurney JJ, Menzies AH, Winter F (2004) An updated classification scheme for mantle-derived garnets, for use by diamond explorers. Lithos 77: 841–857

Hagedorn EM, Boenigk W (2008) The Pliocene and Quaternary sedimentary and fluvial history in the Upper Rhine Graben based on heavy mineral analyses. Neth J Geosci 87: 21–32

Hardman MF, Pearson DG, Stachel T, Sweeney RJ (2018) Statistical approaches to the discrimination of crust- and mantle-derived low-Cr garnet – major-element-based methods and their application in diamond exploration. J Geochem Explor 186: 24–35

Haughton PDW, Farrow CM (1989) Compositional variation in Lower Old Red Sandstone detrital garnets from the Midland Valley of Scotland and the Anglo-Welsh Basin. Geol Mag 126: 373–396

Hieptas J (2012) Investigating the Utility of Detrital Mineral Microchemistry and Radiogenic Isotope Compositions as Provenance Discriminators. Unpublished PhD Thesis, Syracuse University, pp 1–110

Hufmann L (2003) Thermobarometrsiche und geochemische Untersuchungen der Küstenkordillere Chiloés, Südchile. Unpublished PhD Thesis, University of Stuttgart, pp 1–235 (in German with English Abstract)

Hülscher J, Bahlburg H, Pfänder J (2018) New geochemical results indicate a non-Alpine provenance for the Alpine Spectrum (epidote, garnet, hornblende) in Quaternary upper Rhine sediment. Sediment Geol 375: 134–144

Jedlička R, Faryad SW, Hauzenberger C (2015) Prograde metamorphic history of UHP granulites from the Moldanubian Zone (Bohemian Massif) revealed by major element and Y+REE zoning in garnets. J Petrol 56: 2069–2088

Jung S, Hellebrandt E (2006) Trace element fractionation during high-grade metamorphism and crustal melting – constraints from ion microprobe data of metapelitic, migmatitic and igneous garnets and implications for Sm–Nd garnet chronology. Lithos 87: 193–213

Klemd R, Matthes S, Schüssler U (1994) Reaction textures and fluid behaviour in very high-pressure calc-silicate rocks of the Münchberg gneiss complex, Bavaria, Germany. J Metamorph Geol 12: 735–745

Knierzinger W, Wagreich M, Palzer–Khomenko M, Gier S, Meszar M, Lee EY, Koukal V, Strauss P (in print) Provenance and palaeogeographic evolution of Lower Miocene sediments in the eastern North Alpine Foreland Basin. Swiss J Geosci. DOI 10.1007/s00015-018-0312-9

Kohn MJ (2003) Geochemical zoning in metamorphic minerals. In: Rudnick RL, Holland HD, Turekian KK (eds) Treatise on Geochemistry. The Crust. Elsevier–Pergamon, New York, pp 229–261

Krippner A, Meinhold G, Morton A, von Eynatten H (2014) Evaluation of garnet discrimination diagrams using geochemical data derived from various host rocks. Sediment Geol 306: 36–52

Krippner A, Meinhold G, Morton AC, Russell E, von Eynatten, H (2015) Grain-size dependence of garnet composition revealed by provenance signatures of modern stream sediments from the western Hohe Tauern (Austria). Sediment Geol 321: 25–38

Krippner A, Meinhold G, Morton AC, Von Eynatten H (2016) Heavy-mineral and garnet compositions of stream sediments and HP–UHP basement rocks from the Western Gneiss Region, SW Norway. Nor J Geol 96: 7–17

Krogh EJ (1982) Metamorphic evolution of Norwegian country-rock eclogites, as deduced from mineral inclusions and compositional zoning in garnets. Lithos 15: 305–321

Lasaga AC (1984) Chemical kinetics of water-rock interactions. J Geophys Res 89: 4009–4025

Lasaga AC, Soler JM, Burch TE, Nagy KL (1994) Chemical weathering rate laws and global geochemical cycles. Geochim Cosmochim Acta 58: 2361–2386

Locock AJ (2008) An Excel spreadsheet to recast analyses of garnet into end-member components, and a synopsis of the crystal chemistry of natural silicate garnets. Comput and Geosci 34: 1769–1780

Makrygina VA, Suvorova LF (2011) Spessartine in the greenschist facies: crystallization conditions. Geochem Int 49: 209–308

Malvoisin B, Chopin C, Brunet F, Galvez ME (2011) Low-temperature wollastonite formed by carbonate reduction: a marker of serpentinite redox conditions. J Petrol 53: 159–176

Mange MA, Morton AC (2007) Geochemistry of heavy minerals. In: Mange MA, Wright DT (eds) Heavy Minerals in Use. Developments in Sedimentology 58. Elsevier, Amsterdam, pp 345–391

Manning DAC (1983) Chemical variations in garnets from aplites and pegmatites, peninsular Thailand. Mineral Mag 47: 353–358

Mathavan V (1989) A comparative study of compositional zonation in greenschist and granulite facies almandine garnets. J Natl Sci Found Sri Lanka 17: 117–126

Méres Š (2008) Garnets – an important information resource about source area and parent rocks of siliciclastic sedimentary rocks. In: Jurkovič Ľ (ed) Conference "Cambelové dni 2008", Abstract Book. Comenius University, Bratislava, pp 37–43 (in Slovak with English summary)

Méres Š, Aubrecht R, Grdzinski M, Sykora M (2012) High (ultrahigh) pressure metamorphic terrane rocks as the source of the detrital garnets from the Middle Jurassic sands and sandstones of the Cracow Region (Cracow–Wieluń Upland, Poland). Acta Geol Pol 62: 231–243

Morton AC (1985) A new approach to provenance studies: electron microprobe analysis of detrital garnets from Middle Jurassic sandstones of the northern North Sea. Sedimentology 32: 553–566

Morton AC (1987) Influences of provenance and diagenesis on detrital garnet suites in the Fories sandstone, Paleocene, central North Sea. J Sediment Petrol 57: 1027–1032

Morton AC, Hallsworth C (2007) Stability of detrital heavy minerals during burial diagenesis. In: Mange M, Wright DT (eds) Heavy Minerals In Use. Developments in Sedimentology 58. Elsevier, Amsterdam pp 215–245

Morton AC, Hallsworth C, Chalton B (2004) Garnet compositions in Scottish and Norwegian basement terrains: a framework for interpretation of North Sea sandstone provenance. Mar Pet Geol 21: 393–410

Nehyba S, Opletal V (2016) Depositional environment and provenance of the Gresten Formation (Middle Jurassic) on the southeastern slopes of the Bohemian Massif (Czech Republic, subsurface data). Aust J Earth Sci 109: 262–276

Nehyba S, Roetzel R (2010) Fluvial deposits of the St. Marein-Freischling Formation –insights into initial depositional processes on the distal external margin of the Alpine–Carpathian Foredeep in Lower Austria. Aust J Earth Sci 103: 50–80

Neubauer F, Friedl G, Genser J, Handler R, Mader D, Schneider D (2007) Origin and tectonic evolution of the Eastern Alps deduced from dating of detrital white mica: a review. Aust J Earth Sci 109: 8–23

Okay AI (1980) Mineralogy, petrology, and phase relations of glaucophane–lawsonite zone blueschists from the Tavsanh region, northwest Turkey. Contrib Mineral Petrol 72: 234–255

Oliver GJH (2001) Reconstruction of the Grampian episode in Scotland: its place in the Caledonian Orogeny. Tectonophysics 332: 23–49

Otamendi JE, de la Rosa JD, Patiño Douce AE, Castro A (2002) Rayleigh fractionation of heavy rare earths and yttrium during metamorphic garnet growth. Geology 30: 159–162

Paulick H, Franz G (2001) Greenschist facies regional and contact metamorphism of the Thalanga volcanic-hosted massive sulphide deposit (northern Queensland, Australia). Miner Depos 36: 786–793

Pichler H, Schmitt–Riegraf C (1993) Gesteinsbildende Minerale im Dünnschliff. Enke, Stuttgart, pp 1–233 (in German)

Polyakova TN, Savko KA, Skryabin VY (2005) Evolution of early Proterozoic metamorphism within Tim–Yastrebovskaya Paleorift, Voronezh Crystalline Massif, East-European Platform: metapelite systematics, phase equilibrium, and P–T conditions. In: Thomas H (ed) Metamorphism and Crustal Evolution. Atlantic Publishers and Distributors, New Delhi, pp 28–75

Pouchou JL, Pichoir F (1991) Quantitative analysis of homogeneous or stratified microvolumes applied the model "PAP". In: Heinrich KFD, Newbury DE (eds) Electron Probe Quantification. Plenum, New York, pp 31–35

Povondra P, Vrána S (1996) Tourmaline and associated minerals in alkali-feldspar orthogneiss near Hluboká nad Vltavou. J Czech Geol Soc 41: 191–200

Preston J, Hartley AJ, Mange–Rajetzky M, Hole M, May G, Buck S, Vaughan L (2002) The provenance of Triassic continental sandstones from the Beryl Field, Northern Sea: mineralogical, Geochemical, and Sedimentological Constraints. J Sediment Res 72: 18–29

Raič S, Mogessie A, Krenn K, Hoinkes G (2012) Petrology of metamorphic rocks in the Oswaldgraben (Gleinalm Area, Eastern Alps, Styria). Mitt Österr Mineral Gessel 158: 67–81

Roetzel R (2016) Bericht 2010-2014 über geologische Aufnahmen auf Blatt 39. Jb Geo B–A 156: 240–247 (in German)

Roetzel R, Mandic O, Steininger FF (1999) Lithostratigraphie und Chronostratigraphie der tertiären Sedimente im

westlichen Weinviertel und angrenzenden Waldviertel. In: ROETZEL R (ed) Arbeitstagung 1999 Retz–Hollabrunn, Geologische Bundesanstalt, Vienna, pp 38–54 (in German)

RUPP C, LINNER M, MANDL GW (2011) Erläuterungen zur geologischen Karte von Oberösterreich 1:200.000. Geologische Bundesanstalt, Wien, pp 1–255 (in German)

SCHMOLKE MK, BABIST J, HANDY MR, O'BRIEN PJ (2006) The physico-chemical properties of a subducted slab from garnet zonation patterns (Sesia Zone, Western Alps). J Petrol 47: 2123–2148

SCHÖNIG J, MEINHOLD G, VON EYNATTEN H, LÜNSDORF NK (2018) Provenance information recorded by mineral inclusions in detrital garnet. Sediment Geol 376: 32–49

SCHULZE DJ (2003) A classification scheme for mantle-derived garnets in kimberlite: a tool for investigating the mantle and exploring for diamonds. Lithos 71: 195–213

SENGUPTA P, RAITH MM (2002) Garnet composition as a petrogenetic indicator: an example from a marble–calc-silicate granulite interface at Kondapalle, Eastern Ghats Belt, India. Amer J Sci 302: 686–725

SHENBAO D (1993) Metamorphic and tectonic domains of China. J Metamorph Geol 11: 465–481

SHIMAZKI H (1977) Grossular–spessartine–almandine garnets from some Japanese scheelite skarns. Canad Mineral 5: 74–80

SPEAR FS (1995) Metamorphic Phase Equilibria and Pressure–Temperature Time Paths. Mineralogical Society of America, Washington, D.C., pp 1–799

STUTENBECKER L, BERGER A, SCHLUNEGGER F (2017) The potential of detrital garnet as provenance proxy in the Central Swiss Alps. Sediment Geol 351: 11–20.

SUGGATE SM, HALL R (2014) Using detrital garnet compositions to determine provenance: a new compositional database and procedure. In: SCOTT RA, SMYTH HR, MORTON AC, RICHARDSON N (eds) Sediment Provenance Studies in Hydrocarbon Exploration and Production. Geological Society of London, Special Publications 386, pp 373–393

TAKEUCHI M (1994) Changes in garnet chemistry show a progressive denudation of the source areas of the Permian–Jurassic sandstones, southern Kitakami Terrane, Japan. Sediment Geol 93: 85–105

TERAOKA Y, SUZUKI M, HAYASHI T, KAWAKAMI K (1997) Detrital garnets from Paleozoic and Mesozoic sandstones in the Onogawa area, East Kyushu, Southwest Japan. Bull Fac of School Edu, Hiroshima University II 19: 87–101 (in Japanese with English abstract).

THEUNE U (2005) Plot3c. Accessed on January 14, 2019, at *https://de.mathworks.com/matlabcentral/fileexchange/5735-plot3c*

THEYE T, SCHREYER W, FRANSOLET AM (1996) Low-temperature, low-pressure metamorphism of Mn-rich rocks in the Lienne Syncline, Venn-Stavelot Massif (Belgian Ardennes), and the role of carpholite. J Petrol 37: 767–783

TOLOSANO–DELGADO R, VON EYNATTEN H, KRIPPNER A, MEINHOLD G (2018) A multivariate discrimination scheme of detrital garnet chemistry for use in sedimentary provenance analysis. Sediment Geol 375: 14–26

TUCCILLO ME, ESSENE EJ, VAN DER PLUIJM BA (1990) Growth and retrograde zoning in garnets from high-grade metapelites: implications for pressure–temperature paths. Geology 18: 839–842

VON EYNATTEN H, DUNKL I (2012) Assessing the sediment factory: the role of single grain analysis. Earth Sci Rev 115: 97–120

VON EYNATTEN H, GAUPP R, WIJBRANS JR (1996) $^{40}Ar/^{39}Ar$ laser-probe dating of detrital white micas from Cretaceous sedimentary rocks of the Eastern Alps: evidence for Variscan high-pressure metamorphism and implications for Alpine Orogeny. Geology 24: 691–694

VRÁNA S, ŠTĚDRÁ V, NAHODILOVÁ R (2009) Geochemistry and petrology of high-pressure kyanite–garnet–albite–K-feldspar felsic gneisses and granulites from the Kutná Hora Complex, Bohemian Massif. J Geosci 54: 159–179

WELTJE GJ, VON EYNATTEN H (2004) Quantitative provenance analysis of sediments: review and outlook. Sediment Geol 171: 1–11

WENDT AS, D'ARCO P, GOFFE B, OBERHÄNSLI R (1993) Radial cracks around α-quartz inclusions in almandine: constraints on the metamorphic history of the Oman mountains. Earth Planet Sci Lett 114: 449–461

WHITNEY DL, EVANS BW (2010) Abbreviations for names of rock-forming minerals. Amer Miner 95: 185–187

WILLNER AP, PAWLING S, MASSONE HJ, HERVE F (2001) Metamorphic evolution of spessartine quartzites (coti-clues) in the high-pressure, low-temperature complex at Bahia Mansa, Coastal Cordillera of South–Central Chile. Canad Mineral 39: 1547–1569

WIN KS, TAKEUCHI M, TOKIWA T (2007) Changes in detrital garnet assemblages related to transpressive uplifting associated with strike-slip faulting: an example from the Cretaceous System in Kii Peninsula, Southwest Japan. Sediment Geol 201: 412–431

WRIGHT WI (1938) The composition and occurrence of garnets. Amer Miner 23: 436 449

ZEMANN J (1962) Zur Kristallchemie der Granate. Beitr Mineral Petrologie 8: 180–188 (in German)